Molecular Design of Redox Carriers for Electrochemical CO_2 Capture and Concentration

Jeffrey M. Barlow[†1], Lauren Clarke[2†], Zisheng Zhang[3†], Daniel Bím[3], Katelyn Ripley[2], Alessandra Zito[1], Fikile Brushett[2]*, Anastassia N. Alexandrova[3]*, Jenny Y. Yang[1]*

†authors contributed equally

[1] Department of Chemistry, University of California, Irvine, California 92697, United States

[2] Department of Chemistry and Biochemistry, University of California, Los Angeles, Los Angeles, California 90095-1569, United States

[3] Department of Chemical Engineering, Massachusetts Institute of Technology, Cambridge, MA, 02139, United States of America

Corresponding authors: brushett@mit.edu, ana@chem.ucla.edu, j.yang@uci.edu

Abstract

Developing improved methods for CO_2 capture and concentration (CCC) is essential to mitigating the impact of our current emissions and can lead to carbon net negative technologies. Electrochemical approaches for CCC can achieve much higher theoretical efficiencies compared to the thermal methods that have been more commonly pursued. The use of redox carriers, or molecular species that can bind and release CO_2 depending on their oxidation state, is an increasingly popular approach as carrier properties can be tailored for different applications. They key requirements for stable and efficient redox carriers are discussed in the context of chemical scaling relationships and operational conditions. Computational and experimental approaches towards developing redox carriers with optimized properties is also described.

1. Introduction

1.1 Background

Carbon dioxide (CO_2) capture and concentration (CCC) is a foundational technology which, in concert with low-carbon power production, enhanced transmission and distribution, and efficient use, can enable transition to a sustainable global energy economy. The deployment of CCC coupled with sequestration or utilization can immediately address greenhouse gas emissions.[1–3] In the current energy and industrial sectors, post-combustion or post-process capture can be used to remove CO_2 from large volume point sources (i.e., flue gases or effluent gases) following fossil-fuel combustion or chemical transformations in hard-to-decarbonize sectors (e.g., steel and cement industries).[4,5] Other sectors lead to a large quantity of disperse, small volume CO_2

emission streams (e.g., transportation, residential, and agricultural) that can also be mobile, and thus challenges the use of point source capture approaches. In such cases, direct air capture (DAC), where CO_2 is separated from ambient air, may be the best method for carbon emissions management. Operation of DAC in the long-term can also lead to net-negative operation.[6,7] At present, a number of global CCC projects are operational, under development, or in construction, for both post-combustion capture and DAC.[8] While candidate CCC technologies have been demonstrated at relevant scales, widespread implementation is largely limited by technical and economic factors. The most significant barrier is the high energetic requirements of current systems, which in turn leads to high capital and operating costs.[5,6,9–11] Ultimately, the mechanism of CO_2 capture and release will define system energetics and overall process costs.

The most common approaches for both post-combustion capture and DAC employ thermally-driven chemical absorption (adsorption) cycles, where a solvent (sorbent) is used to bind CO_2, effectively removing it from a feed gas stream, followed by an input of heat as the primary driving force for solvent (sorbent) regeneration and CO_2 recovery at higher concentrations [5,6] The key challenge in using heat for CO_2 capture and release is that the two components of free energy, enthalpy and entropy, make opposing contributions in each step. CO_2 capture is entropically unfavorable; therefore, capture of dilute CO_2 requires sufficiently large negative sorbent reaction enthalpies (i.e., large binding affinities). However, the large reaction enthalpies required for capture hamper CO_2 release. Since release is entropically favorable, elevated temperatures are required to offset the large negative enthalpic contribution. As such, temperature-driven CO_2 absorption or adsorption systems have high heating demands during regeneration, particularly from dilute feed streams such as air. Current processes operate with low energetic efficiencies of ca. 5-30%, even after optimization at scale.[12–16] These lower energetic efficiencies limit the potential for cost reduction in thermochemical CO_2 capture systems.

Although less mature, the use of electrochemical CCC (eCCC) cycles to separate CO_2 has the potential to address the inherent limitations of thermochemically-based absorption or adsorption processes. Use of electrochemistry can enable high energetic efficiencies, safe operation at mild conditions (closer to ambient temperature and pressure), and direct coupling with renewable energy sources. Electrochemical technologies are also modular, and thus can be scaled down more readily than thermochemical processes, which may permit cost-effective capture from small/disperse emissions.[17–21]

A variety of electrochemical methods for CO_2 capture have been pursued, starting in the late 1960's,[22] where the use of molten salt electrolysis was proposed to maintain CO_2 levels in sealed close-quarter vessels such as submarines, aircraft, or spacecraft.[23–27] The cost of electricity (as compared to heat) likely limited large scale technology deployment and restricted use to niche applications where efficiency and compactness superseded cost.

Recently, there has been renewed interest in employing electrochemical approaches for carbon capture, and broadly across industry, due to *(1)* the increasing urgency to meaningfully address CO_2 emissions to avoid the worst effects of climate change and *(2)* the emergence and expansion of low-cost carbon-free renewable electricity enabled by increasing deployments of solar and wind technologies. As a result, this field has expanded to include MOFs,[28–31] electrochemically mediated amine regeneration (EMAR),[32–37] as well as the utilization of bipolar membranes[38] or proton coupled electron transfer (PCET) mediators[39–45] which induce pH changes in aqueous solutions to facilitate CO_2 uptake and release. In addition to these methods, there has been increasing interest in the utilization of redox-active capture molecules to directly bind and release CO_2, which is the focus of this tutorial review. In these direct eCCC systems, redox-active sorbents can be solubilized (dissolved in an electrolyte) or immobilized (embedded on an electrode surface). While there are similarities between design considerations for both approaches, here we specifically consider the case of solubilized sorbents, which can also be referred to as redox carriers. For these systems, the design of redox carriers with desirable properties is essential for developing cost-competitive and long-lasting technologies with high energetic efficiency, CO_2 selectivity, separation capacity, and sorbent stability. To this end, this tutorial review seeks to describe the basics of eCCC systems, outline design criteria for redox carriers and system requirements, survey redox carrier molecules and observed trends, and highlight opportunities for scientific and engineering advancement through the lens of molecular design.

1.2 Thermodynamic Considerations for eCCC Processes

For any CCC approach, the minimum thermodynamic work required to concentrate CO_2 from an ideal gaseous mixture is governed by the standard Gibbs free energy difference, $\Delta G_{\min}$ (J mol^{-1} CO_2), for a specific shift in equilibrium. For removing an infinitesimal quantity of CO_2, such that the bulk composition remains unaltered, this thermodynamic limit is given by the following equation.[46]

$$\Delta G_{\min} = RT\ln\left(Q_{\mathrm{CO_2}}\right) \quad \text{where } Q_{\mathrm{CO_2}} = \frac{P_{\mathrm{CO_2,f}}}{P_{\mathrm{CO_2,i}}} \qquad \mathbf{1}$$

Here, R is the ideal gas constant (8.314 J mol^{-1} K^{-1}), T is the absolute temperature (K), and Q_{CO2} is the reaction quotient (-) for the CO_2 concentration process. The partial pressures of CO_2 in the initial and final mixtures are denoted by $P_{\mathrm{CO_2,i}}$ and $P_{\mathrm{CO_2,f}}$. This relationship between the change in free energy and reaction equilibria in equation 1 indicates that the process of concentrating CO_2 is endergonic and is dependent upon the desired changes in concentration and system temperature. For context, Table 1 shows the minimum work required to concentrate CO_2 into a pure stream (100% CO_2 or $P_{\mathrm{CO_2,f}}$ = 1 atm) at standard temperature (T = 298 K) from a variety of application-relevant initial concentrations ($P_{\mathrm{CO_2,i}}$). The data from Table 1 shows that more energy is needed to concentrate CO_2 from more dilute sources; for instance, it requires more than 4× the energy to capture CO_2 from the atmosphere (0.04% CO_2)[47] as compared to flue gas from a coal-fired power plant (15% CO_2)[47], with 19.4 and 4.7 kJ mol^{-1} CO_2 required, respectively. The minimum energy requirements also increase as the fraction of CO_2 captured deviates from 0 and more than an infinitesimal quantity of CO_2 is removed. For example, when 90% of CO_2 is captured from flue gas (15% CO_2), $\Delta G_{\min}$ increases to 6.4 kJ mol^{-1} CO_2 (calculated using equations derived by Lackner).[46]

For electrochemically-mediated processes, the capture and release cycles are initiated by applying a potential or bias to an electrode instead of the changes in temperature that are used in thermally-driven systems. The electrochemical bias at the electrode surface results in oxidation or reduction of species in solution that captures or releases CO_2 in the solution or material surface(s) to carry out the CCC process. The change in the Gibbs free energy, ΔG (J mol^{-1}), for an electrochemical process is thus related to the cell potential, E_{cell} (V) and computed $\Delta G_{\min}$ and $E_{\min}$ requirements for the associated eCCC processes, as described in Table 1. It is assumed that CO_2 is recovered at 100% purity ($P_{\mathrm{CO_2,f}}$ = 1 atm) and the redox carrier can theoretically capture one CO_2 molecule for every electron transferred ($n/q = 1$).

Table 1. Representative CO_2 partial pressures of various sources ($P_{\mathrm{CO_2,i}}$),[5,47–50] and computed $\Delta G_{\min}$ and $E_{\min}$ requirements for the associated eCCC processes. It is assumed that CO_2 is recovered at 100% purity ($P_{\mathrm{CO_2,f}}$ = 1 atm) and the redox carrier can theoretically capture one CO_2 molecule for every electron transferred ($n/q = 1$).

Application	$P_{CO_2,i}$ (atm)	ΔG_{min} (kJ mol^{-1} CO_2)	$\lvert E_{min} \rvert$ (mV)
Direct air capture	4.0×10^{-4}	19.4	201
Transportation (i.e. passenger cabin)	1.0×10^{-3}	17.1	177
Aluminum production (flue gas)	0.01	11.4	118
Natural gas fired boiler (flue gas)	0.10	5.7	59
Oil-fired boiler (flue gas)	0.12	5.3	54
Coal-fired boiler (flue gas)	0.15	4.7	49
Steel production (flue gas)	0.20	4.0	41
Cement production (flue gas)	0.30	3.0	31
Biogas purification	0.50	1.7	18
Ethanol production	0.90	0.3	3

While $E_{\min}$ is relatively low, this represents the minimum potential required for separation, and the actual cell voltage will be larger due to concentration changes during operation and cell overpotentials, as described in Section 1.5. The extent of the deviation in the cell voltage from $E_{\min}$ will be dictated by properties of the sorbent chemistry as well as process design aspects. Thus, for direct eCCC systems, redox carrier design *and* process engineering will be important to achieve optimal properties for efficient separations.

1.3 Overview of eCCC with Redox Carriers

A redox carrier for CO_2 must be able to reversibly bind CO_2 in one oxidation state and release it in another as shown in Scheme 1. Typically, the resting state carrier (R) is reduced with n electrons to form the active state carrier species $(R)^{n-}$ at a reduction potential (i.e., standard reduction potential), $E_{1/2(\mathrm{cap})}$. The reduced species has a high affinity for CO_2 ($K_{CO_2(R^{n-})}$), and can bind q CO_2 molecules, which allows capture from a dilute inlet stream to form the CO_2-bound adduct, $R(CO_2)_q^{n-}$. CO_2 release is triggered by oxidation of $R(CO_2)_q^{n-}$ to form $R(CO_2)_q$, which is characterized by $E_{1/2(\mathrm{rel})}$. The oxidized carrier has a much lower affinity for CO_2 ($K_{CO_2(R)}$), resulting in liberation of q CO_2 to reform the resting-state carrier (R) and complete the cycle. This approach takes advantage of the difference between the CO_2 binding affinities of the oxidized, $K_{CO_2(R)}$, and reduced, $K_{CO_2(R^{n-})}$, states of the carrier (R and R^{n-}, respectively). While we specifically discuss systems that employ solubilized redox carriers, Scheme 1 is also representative of eCCC with immobilized, redox-active sorbents. We also note that the reaction

mechanism shown in Scheme 1 is simplified; in reality, carriers may undergo multiple electron transfer events and bind CO_2 at each associated oxidation state, which is discussed in more detail in Section 2.1.

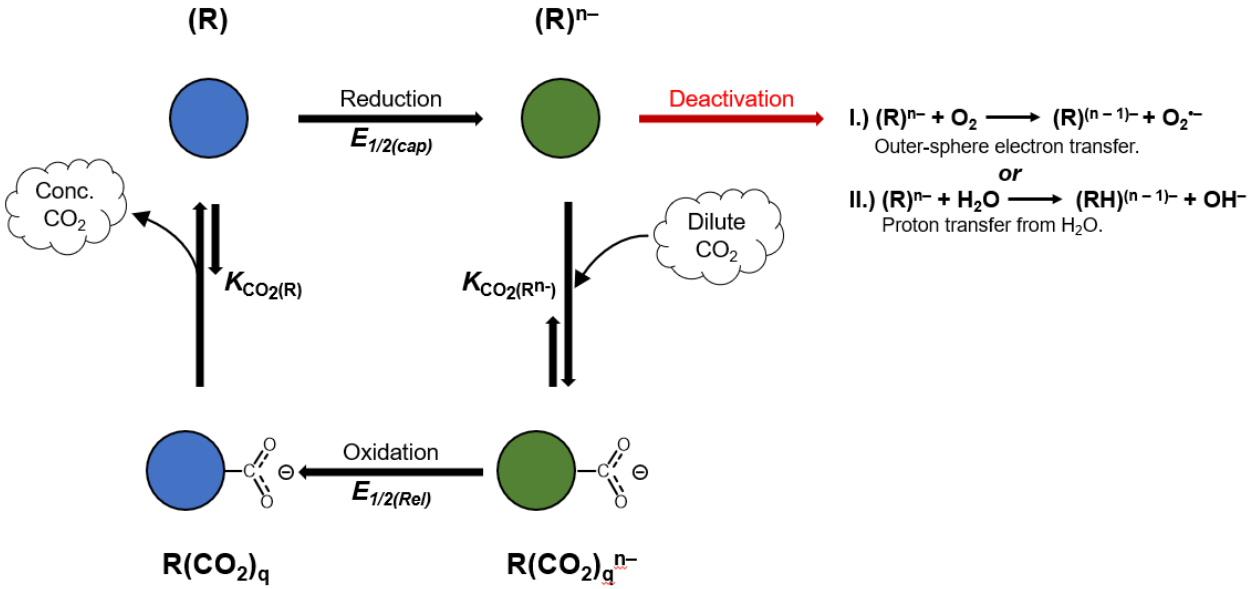

Scheme 1. General process for eCCC systems featuring a redox carrier (R, top left). (R), which has a small or negligible binding constant for CO_2 ($K_{CO2(R)}$), is reduced at the cathode at $E_{1/2(cap)}$ potential to yield $(R)^{n-}$, which has a higher binding constant for CO_2 ($K_{CO2(Rn-)}$). The reduced carrier $(R)^{n-}$ selectively binds CO_2 from a dilute gas stream, forming $R(CO_2)_q^{n-}$. Regeneration of the carrier is accomplished by oxidation of $R(CO_2)_q^{n-}$ to $R(CO_2)_q$ at the anode at $E_{1/2(rel)}$ leading to release and concentration of CO_2 and regeneration of the neutral state of the redox agent (R). In this scheme, n represents the stoichiometric ratio of moles of electrons transferred per mole of CO_2. (Right, in red) Two reactions with O_2 and H_2O that can deactivate $(R)^{n-}$: 1) If the $E°_{cathodic}$ potential is more negative than the $O_2/O_2^{\bullet-}$ reduction potential, electron transfer from $(R)^{n-}$ to O_2 to form superoxide can occur. 2) If the pK_A of $(RH)^{(n-1)}$ is higher than the pK_A of water or protic solvent, protonation of $(R)^{n-}$ can occur.

1.4 System Configurations for eCCC with Redox Carriers

While dominant process designs have yet to emerge due to the relative nascency of the field, multiple groups have considered different design strategies for electrochemical CO_2 separators,[32,39,51,52] which can be broadly categorized into four system configurations. Figure 1 presents envisioned examples of each configuration for continuous eCCC systems based on

solubilized redox carriers. A 4-stage system (Figure 1(a)) employs an electrochemical cell for carrier activation (cathode) and deactivation (anode). CO_2 dissolution and absorption, following carrier activation, primarily occurs in a separate process unit such as an absorption column. Similarly, CO_2 desorption and degasification are carried out in a separate process step after deactivation. A mode for CO_2 removal can be incorporated into the anode design, which is referred to as anodic desorption. This allows for simultaneous carrier deactivation, CO_2 desorption, and degasification, which eliminates the need for a separate desorption unit. Adoption of anodic desorption in the system is classified as a 3-stage configuration (Figure 1(b)). A 3-stage configuration can instead incorporate cathodic absorption (Figure 1(c)), where the CO_2-containing feed gas is contacted with the carrier within the cathode compartment. This cathode design allows for simultaneous carrier activation, CO_2 dissolution, and CO_2 absorption. Finally, a 2-stage configuration integrates both anodic desorption and cathodic absorption, such that all phenomena occur within the electrochemical cell (Figure 1(d)). This type of system could potentially be operated without the need for liquid pumping. In this format, the carrier-containing electrolyte can be enclosed within the inter-electrode gap, either as a free liquid volume, imbibed into a porous separator, or absorbed into a membrane. Notably, a 2-stage configuration has also been demonstrated with immobilized redox-active sorbents on a working electrode, paired with a counter electrode that serves as a source and sink of electrons.[53,54] This cell format necessitates batch (i.e., electro-swing[55]), rather than continuous operation, where the working electrode is cycled between the CO_2 capture and release stages.

Prior work has demonstrated that each of the considered configurations can lead to significant differences in performance. Thermodynamic modeling shows that 2-stage systems can operate at the highest energetic efficiency and approach the thermodynamic limit for energy requirements ($\Delta G_{\min}$). More generally, implementation of cathodic absorption and/or anodic desorption reduces the thermodynamic driving force for capture and release, leading to greater reversibility and resulting in higher energetic efficiencies.[52,56] However, system design decisions should not be based on this thermodynamic argument alone. For example, operation of a system with a reduced driving force for binding and/or release will occur at a slower rate. In a system with cathodic absorption, this will manifest as current density limitations, as operation of the electrochemical cell will likely be restricted by mass transport of CO_2 from the feed gas to the reaction environment. Thus, it is likely that operating current densities for configurations with cathodic absorption will

be lower, especially for capturing CO_2 from dilute sources, leading to higher electrochemical reactor costs. There are other aspects to consider as well which may not be specifically linked to performance. For example, a 4-stage system makes use of process units that are commonly employed and well understood in industry (i.e. absorption columns and flash tanks), and therefore implementation of this configuration may be beneficial for post-combustion capture from industrial sources and power plants. Comparatively, a 2-stage system can embody a more simplified and modular process scheme with no liquid circulation. This may be advantageous for DAC applications which do not have requirements for process size and may be operated in remote locations. Overall, four general configurations have been considered thus far, which will each have inherent advantages and disadvantages, and thus each may be more beneficial in different applications. While choice of configuration in itself can impact performance, this is also innately linked with molecular properties. More generally, molecular properties impact process performance, and the resulting trends are different for each configuration, which is described in more detail in the following section.

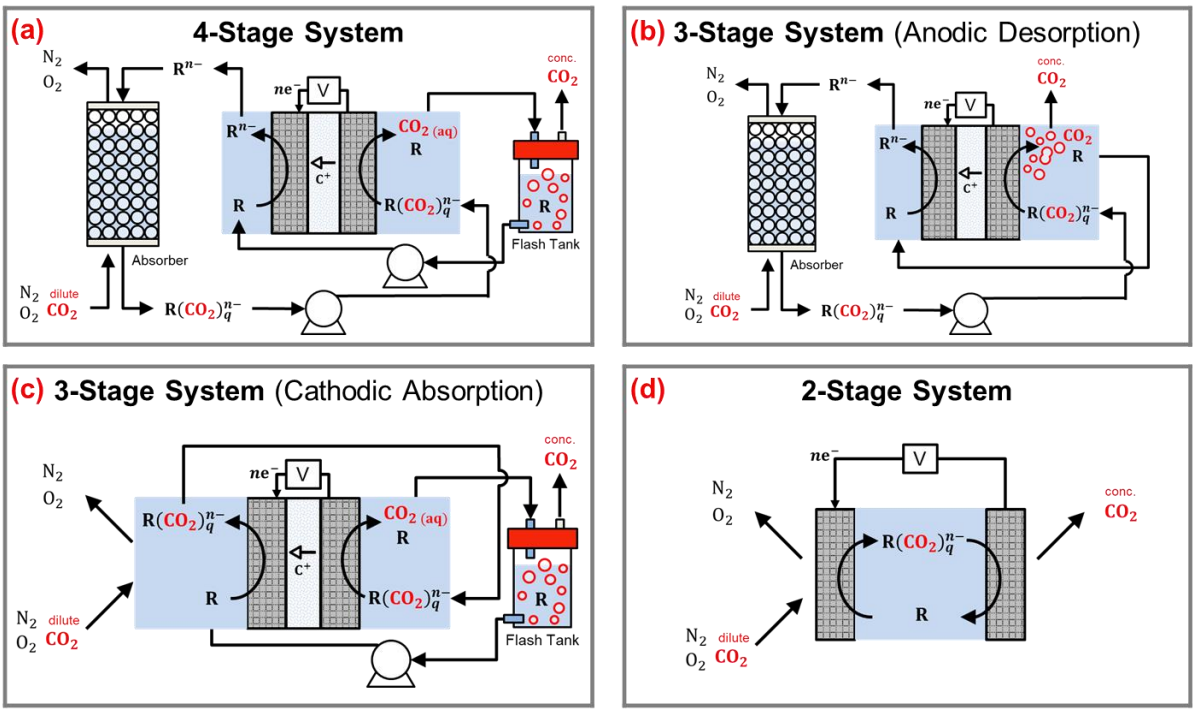

Figure 1. Potential embodiments of four eCCC configurations leveraging dissolved redox carriers: (a) 4-stage system, (b) 3-stage system with anodic desorption, (c) 3-stage system with cathodic absorption, and (d) 2-stage system. Figure adapted from Ref.[52,56].

1.5 General Requirements for eCCC with Redox Carriers

For redox carriers, there are general criteria which can enable high performance eCCC systems if achieved. The ideal redox carrier should have high affinity for CO_2 binding when activated, complete CO_2 release when deactivated, high solubility, high CO_2 selectivity, and long-term stability. These characteristics will enable sorbents with long lifetimes and high CO_2 separation capacities, reducing the required cost of materials and chemicals. Additionally, the ideal carrier and electrolyte pair should permit fast mass transport and kinetics, operation at low cell voltages, and high current densities. Such conditions will minimize costs associated with both energy and materials.

High CO_2 binding affinity and complete release is important for achieving high separation capacities due to the impact on faradaic efficiency (defined here as moles of CO_2 separated per mole of electrons transferred). Achievement of these properties will be dictated by binding constants in the activated and deactivated states $K_{CO_2(R^{n-})}$ and $K_{CO_2(R)}$, respectively, for the simplified mechanism in Scheme 1. Specifically, $K_{CO_2(R^{n-})}$ must be high enough to capture CO_2 from a given feed gas composition and $K_{CO_2(R)}$ must be low enough to permit the complete release of CO_2. For example, previous work has estimated that CO_2 capture at high faradaic efficiencies from flue gas (15% CO_2) requires $K_{CO_2(R^{n-})} > \sim 10^3$–$10^4$, whereas DAC would need $K_{CO_2(R^{n-})} > \sim 10^5$–$10^6$, both with the requirement that $K_{CO_2(R)} < \sim 1$.[52,57] However, we note that these estimates are used for demonstration and should not be taken as exact guidelines, since specific values of required binding coefficients will change depending upon other process factors, such as electrolyte properties (e.g., carrier concentration and CO_2 solubility), operating parameters (e.g. state of charge swing and % CO_2 removal), and system configuration. These $K_{CO_2(R^{n-})}$ and $K_{CO_2(R)}$ estimates were made assuming a 1 M carrier concentration, a CO_2 solubility in the range of 0.01–0.3 M atm^{-1}, and use of a carrier that can bind one CO_2 molecule (q = 1). If the carrier concentration is decreased (relative to the CO_2 solubility), for example, required $K_{CO_2(R^{n-})}$ values would be higher, and faradaic efficiencies would also be reduced. These estimates also do not consider the fraction of CO_2 that is removed from the feed gas. In general, ideal redox carriers should have sufficient binding affinities ($K_{CO_2(R^{n-})}$ and $K_{CO_2(R)}$), as well as high carrier concentration (both absolute and relative to CO_2 solubility), to enable operation at high separation capacities and faradaic efficiencies. The ideal properties identified

here were based upon maximization of the faradaic efficiency, although this is not the only important performance metric. Prior work indicates that systems lacking cathodic absorption (e.g., 4-stage system) may benefit from lower $K_{CO_2(R^{n-})}$ values (which do not maximize the faradaic efficiency) due to an inherent tradeoff between faradaic and energetic efficiency in these systems.[52]

The cell voltage (V_{cell}) can be generally represented as an equilibrium potential difference (E_{cell}) with the addition of overpotentials due to kinetics (η_s), mass transport (η_{conc}), and ohmics (η_{ohm}). This relation is shown in equation 3 for an electrolytic device.[58]

$$|V_{cell}| = |E_{cell}| + |\eta_s| + |\eta_{conc}| + |\eta_{ohm}| \quad \textbf{3}$$

For operation at low cell voltages, overpotentials resulting from kinetics, mass transport, and ohmics should be minimized. This goal may be achieved with high carrier solubilities (permitting high concentrations), fast electrochemical kinetics, high diffusivities, and a highly conductive electrolyte. These properties may also permit operation at high current densities.

The equilibrium potential difference also impacts the cell voltage, and thus, should also be minimized. This potential, E_{cell}, is equal to the equilibrium potential difference between the cathode and anode. In an ideal system with a symmetric cell (as shown in Figure 1), the cathode will only carry out the carrier activation reaction for CO_2 capture, and the only reaction at the anode will be the carrier deactivation for CO_2 release. Thus, the equilibrium potentials for the cathode and anode can be represented with the Nernstian potentials for the activation (for capture) and deactivation (for release) reactions, which we define here as E_{cap} and E_{rel}, respectively. For ideal solutions, the equilibrium potentials, E_{cap} and E_{rel}, will be related to the standard reduction potentials, $E_{1/2(cap)}$ and $E_{1/2(rel)}$, and species concentrations (bracketed, mol L^{-1}) according to the Nernst equation, as shown in equations 4 and 5 for the Scheme 1 mechanism.

$$E_{cap} = E_{1/2(cap)} - \frac{RT}{nF}\ln\left(\frac{[R^{n-}]}{[R]}\right) \quad \textbf{4}$$

$$E_{rel} = E_{1/2(rel)} - \frac{RT}{nF}\ln\left(\frac{[R(CO_2)^{n-}]}{[R(CO_2)]}\right) \quad \textbf{5}$$

Thus, the equilibrium potential difference, E_{cell}, may be impacted by the reduction potentials, $E_{1/2(cap)}$ and $E_{1/2(rel)}$. More specifically, a larger difference between the reduction potentials ($\Delta E_{1/2} = E_{1/2(rel)} - E_{1/2(cap)}$) of the electrochemical reactions can lead to high cell voltages and

reduced energetic efficiencies. Ideally, low $\Delta E_{1/2}$ would be preferred; however, this is challenged by an intrinsic relation between $K_{CO_2(R^{n-})}/K_{CO_2(R)}$ and $\Delta E_{1/2}$ (equation 6).

$$\Delta E_{1/2} = \frac{RT}{nF} \ln\left(\frac{K_{CO_2(R^{n-})}}{K_{CO_2(R)}}\right) \quad \textbf{6}$$

From a thermodynamic perspective, a larger $K_{CO_2(R^{n-})}/K_{CO_2(R)}$ ratio can increase the driving force for CO_2 capture and release, which consequently introduces irreversibility into the system, resulting in larger cell voltages and thus lower energetic efficiencies. As a result, any thermodynamic driving force beyond the minimum required $K_{CO_2(R^{n-})}/K_{CO_2(R)}$ for a specific concentration swing may negatively impact system energetics. However, it has also been shown that this is dependent upon the choice of system configuration.[51,56,59] For systems which implement both cathodic absorption and anodic desorption (i.e., a 2-stage system), where CO_2 is fed to and removed from the electrodes, the thermodynamic driving force for capture and release is reduced (even at high $K_{CO_2(R^{n-})}/K_{CO_2(R)}$ ratios). Considering the electrode potentials, the increase in $\Delta E_{1/2}$ due to higher values of $K_{CO_2(R^{n-})}/K_{CO_2(R)}$ is offset by favorable Nernstian potential shifts due to CO_2 binding at the cathode and CO_2 removal at the anode. For the configurations which lack cathodic absorption and/or anodic desorption, increasing the $K_{CO_2(R^{n-})}/K_{CO_2(R)}$ ratio can result in lower energetic efficiencies due to the inherently higher $\Delta E_{1/2}$. This consideration is a vital factor in the design of redox carriers (and the overall system). For example, a carrier capable of CO_2 concentration from atmospheric sources could theoretically be used to concentrate from flue gas. However, the latter system may operate at a lower efficiency due to this increased standard reduction potential difference.

Finally, the carrier should be selective towards CO_2 and stable in both oxidized and reduced states. High selectivity and stability require the carrier to preferentially bind CO_2 in its activated state and avoid side reactions which can lead to undesirable side products and/or species decay. A current challenge within the field is that carriers that are reduced in their activated state tend to react with dioxygen (O_2) and/or water vapor (H_2O) (Scheme 1).[60] For the former, the reduced carrier can participate in redox chemistry with O_2, the most common of which is a one electron transfer event to re-generate the resting state (R) while also forming superoxide (O_2^-) (Scheme 1, equation I), reducing the overall faradaic efficiency for CO_2 capture. Perhaps more deleterious, the superoxide species can react irreversibly with the carrier, solvent, or electrolyte, negatively impacting long-term cycling stability.[61,62] If the reduced carrier is sufficiently basic, it can also be

protonated by from water or other acidic protons in the solvent/carrier, reducing the carrier's propensity to capture CO_2 (Scheme 1, equation II).[63]

In both atmospheric and industrial CO_2 capture applications, O_2 and H_2O may be present in large quantities. While pre-treatment of inlet gas streams is possible to preclude O_2 and protonation sources, their implementation typically results in increased costs and decreased energetic efficiencies; thus, ideal carriers should be tolerant to O_2 and H_2O. The thermodynamic favorability for an electron transfer to O_2 (equation 7) is dictated by the standard reduction potential of the carrier ($E_{1/2(\mathrm{cap})}$ in the simplified mechanism) as compared to the $O_2/O_2^{\bullet-}$ couple, ($E_{1/2(O_2/O_2^{\bullet-})}$) which typically occurs at ~ –1.2 V vs $Fe(C_5H_5)_2^{+/0}$ in organic solvents.[64,65] The free energy of a protonation event, as shown in equation 8, is dictated by the pK_a of $(RH)^{(n-1)-}$. More generally, the favorability of protonation is governed by the pK_a of the CO_2-binding site of a carrier as compared to the pK_a of other sites in the molecule, water, and/or protic media. Therefore, an optimal redox carrier for eCCC will have low pK_a and more positive $E_{1/2(\mathrm{cap})}$ values. However, as we describe in the following section, correlations exist between these properties and the CO_2 binding affinity, which challenge the achievement of these ideal conditions.

Overall, these are the requirements that must be considered for high performance operation of eCCC systems. There are also many process factors which can be changed to improve performance, including molecular properties, operating conditions, and system design. However, this tutorial review will focus specifically on the molecular design of redox carriers by tuning the CO_2 binding affinity, standard reduction potential, and pK_a. We describe the inherent relationships between these properties as well as how they may be impacted by the solvent environment. We outline approaches to designing redox carriers which have adequate CO_2 binding at mild potentials and low pK_a values, and describe how theory and computational methods can be used to supplement and accelerate this design process.

2. Survey of Redox Carrier Molecules

To be considered as a candidate CO_2 redox carrier, a molecule must contain both a CO_2-binding site and a redox-active site. CO_2 binding is associated with a pronounced reorganization in the CO_2 geometry, changing from a linear to a bent structure. In most cases, a neutral CO_2 molecule binds via the electrophilic carbon atom to an electron-rich nucleophilic center, such as

a metal to form a metal carboxylate, an alkoxide to form a carbonate, or an amide to form a carbamate. Thus, for these redox carrier systems, the redox-active site must induce a substantial change in electron localization (i.e., electron density) at the CO_2-binding site to enhance (or decrease) its nucleophilicity, and therefore, binding.[60,66] The redox-active and binding sites can be the same (co-located) or distinct; however, if the two sites are separated, reduction (or oxidation) at the redox-active site must generate this change in electron density as described above.[60,66] Early studies noted the importance of proximity of the redox center to the CO_2 binding site, where it was found that shorter distances between the two sites resulted in larger binding affinity differences between the activated and deactivated states of the carrier.[67] The observed differences in CO_2 binding between different oxidation states of a carrier were negligible when the sites were separated by more than a single atom, emphasizing the importance of electronic communication between the two sites.

Several classes of organic molecules and transition metal complexes meet this requirement of having both a redox-active and CO_2 binding site, and have been assessed for their potential capabilities as a redox carrier for eCCC. Among the organic compounds, thiols,[68,69] bipyridines,[70–72] and quinones have all demonstrated capabilities for eCCC; however, quinones are currently the most widely explored family of redox carrier molecules and therefore will be a main focus of this tutorial review. Observed trends for previously reported carriers will be discussed in the following sections. First, correlations between redox-carrier CO_2 binding affinity and reduction potential, are discussed for quinones (Section 2.1) and transition metal complexes (Section 2.2). We then assess what these correlations imply for the design of effective yet stable redox carriers (Section 2.3).

2.1 *Quinones (Organic Redox Carriers)*

Correlation Between CO_2 Binding (K_{CO_2}) and Reduction Potential ($E_{1/2}$). In neutral aprotic media, quinones (**Q**) typically undergo two sequential one-electron transfer events (n = 2 in Scheme 1). The quinone is first reduced to generate a semiquinone or radical anion ($\mathbf{Q_{RA}}$), and this reaction is characterized by a reduction potential, $E_{1/2(\mathrm{Q/Q_{RA}})}$ in Scheme 2. The radical anion undergoes its second reduction step to form a dianion ($\mathbf{Q_{DA}}$), at a more negative reduction potential, $E_{1/2(\mathrm{Q_{RA}/Q_{DA}})}$.[73] Previous work in eCCC has shown that quinones can bind CO_2 at one or both of the anionic oxygen sites following reduction, corresponding to q = 1 or 2 in the

generalized reaction network shown in Scheme 1. More specifically, it has been proposed that a quinone binds CO_2 via an ECEC or EEC mechanism, where E denotes an electron transfer step, C indicates a chemical step, and the notation indicates the order of these steps in the mechanism.[49,51,52,74] The disparity in mechanism likely arises from the thermodynamic favorability of CO_2 binding to a quinone radical anion species (**Q_{RA}**), which is defined by the CO_2 binding affinity for **Q_{RA}**, $K_{CO_2(RA)}$. If CO_2 binds upon formation of **Q_{RA}** (ca. $K_{CO_2(RA)} >> K_{CO_2(Q)}$ prior to further reduction to **Q_{DA}**, then an ECEC mechanism would predominate. However, if CO_2 binding to **Q_{RA}** is unfavorable (ca. $K_{CO_2(RA)} \sim K_{CO_2(Q)}$), then an EEC mechanism would occur. A complication to this assessment, however, is if disproportionation of two **Q_{RA}** molecules transpires to create **Q** and **Q_{DA}**, which then reacts with CO_2, as shown at the top of Scheme 2.[66,75,76] Disproportionation would result in inflated values for $K_{CO_2(RA)}$ and may falsely suggest an ECEC mechanism if not properly considered.

Scheme 2.

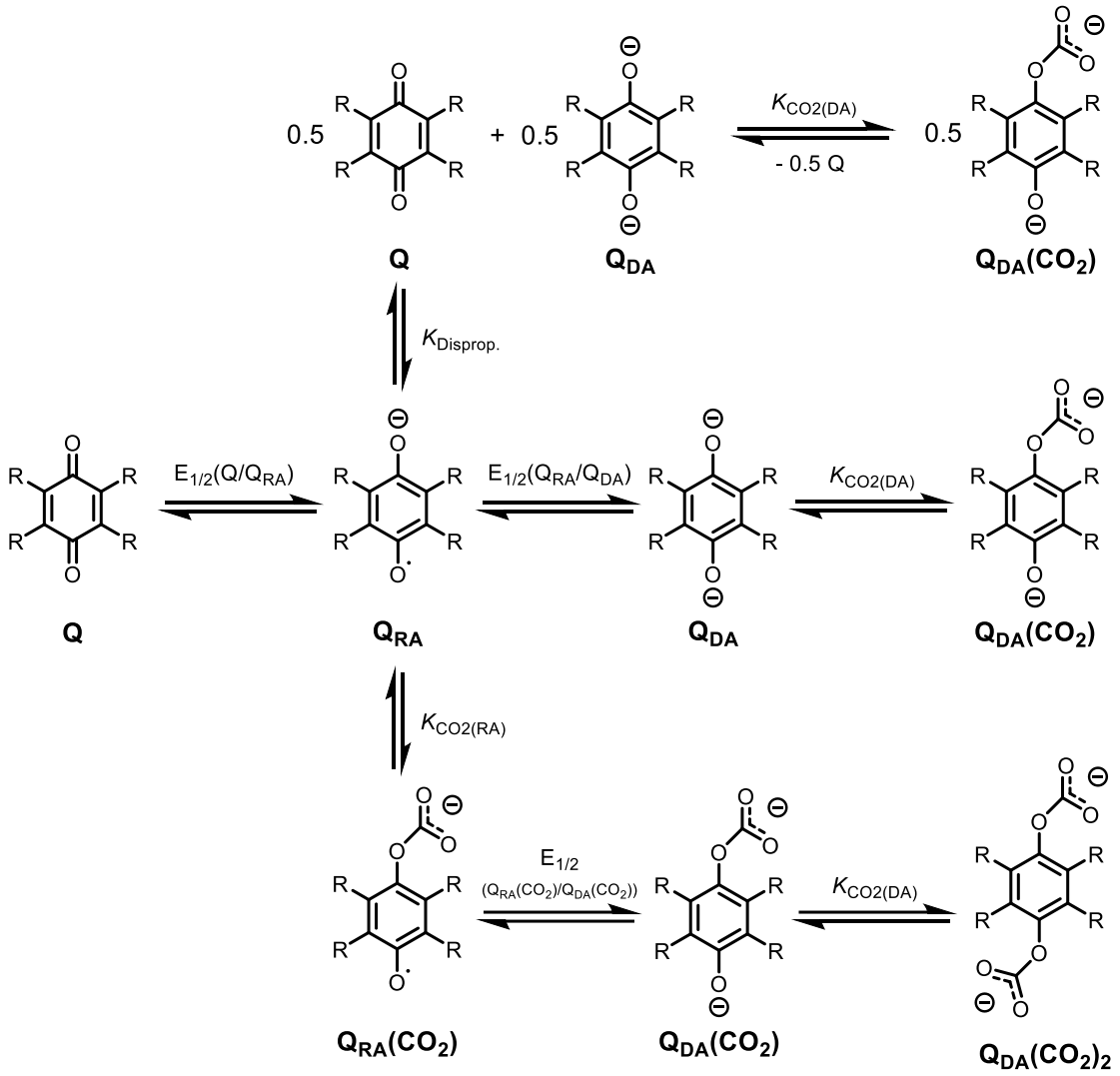

Quinones have an affinity for CO_2 in their reduced forms (**Q_{DA}** and sometimes **Q_{RA}**). Reported CO_2 binding constants with quinone dianions ($K_{CO_2(DA)}$) have been shown to vary between < 10 to > 10^{18} (Table 2).[63,66,67] Although, numerous quinones have been observed to bind CO_2 in their radical anion state (**Q_{RA}**), only two values for $K_{CO_2(RA)}$ have been reported to date, for PAQ and DtBBQ.[66,67] These reported binding constants for both radical anions ($K_{CO_2(RA)}$) were several orders of magnitude smaller than the corresponding values for the dianions ($K_{CO_2(DA)}$). Although no other values of $K_{CO_2(RA)}$ have been quantitatively determined, studies by cyclic voltammetry suggest that $K_{CO_2(RA)}$ is usually much smaller than $K_{CO_2(DA)}$.[63,66,67,77–79] The disparity between CO_2 binding of each species is likely due to increased nucleophilicity of the oxygen atoms in the dianion.

Table 2. Reported reduction potentials of various quinones in N_2 ($E_{1/2(Q_{RA}/Q_{DA})}$) and CO_2 ($E'_{1/2(Q_{RA}/Q_{DA})}$) environments, and measured CO_2 binding coefficients of the dianion, $K_{CO_2(DA)}$.

Quinone	Solvent	$E_{1/2(Q_{RA}/Q_{DA})}$ (N_2)†	$E'_{1/2(Q_{RA}/Q_{DA})}$ (CO_2)†	$\Delta E_{1/2}$[a]	$\ln(K_{CO_2(DA)})$	Ref.
Tetrachloro- 1, 4-benzoquinone (TCQ)	DMF	–0.72	N/A	N/A	3.8	[29]
2, 6-di-*tert*-butyl-1, 4-benzoquinone (DtBBQ)	DMF	–1.46	N/A	N/A	15.0	[29]
Phenanthrenequinone (PAQ)	DMF	–1.19	N/A	N/A	11.8	[29]
2, 3-dicyano-1, 4-benzoquinone*	DMF	–0.47	N/A	N/A	3.8	[29]
Tetrafluro-1, 4-benzoquinone (TFQ)	DMF	–0.80	–0.50	0.30	4.3	[47]
1, 4-benzoquinone (BQ)*	DMSO	–1.05	0.00	1.05	16.9[b]	[48]
Anthraquinone (AQ)	DMSO	–1.40	–0.65	0.75	11.8[b]	[48]
Duroquinone (DQ)	DMSO	–1.55	–0.33	1.22	19.9[b]	[48]
Napthoquinone (NQ)	DMSO	–1.25	–0.40	0.85	13.5[b]	[48]
2, 6-dimethyl- 1, 4-benzoquinone (DMBQ)	DMSO	–1.40	–0.23	1.17	19.0[b]	[48]
2, 6- dichloro- 1, 4-benzoquinone	MeCN	–0.94	–1.00	0.34	6.0	[49]
2- chloro- 1, 4-benzoquinone	MeCN	–1.07	–0.58	0.49	10.0	[49]
Tetrafluro-1, 4-benzoquinone (TFQ)	MeCN	–0.80	–0.62	0.18	3.8	[49]
Tetrachloro- 1, 4-benzoquinone (TCQ)	MeCN	–0.74	–0.63	0.11	2.5	[49]
5-Hydroxy-napthoquinone**	MeCN	–0.94	–0.71	0.23	3.3	[49]
1, 8- dihydroxy-anthraquinone**	MeCN	–1.20	–0.94	0.26	5.4	[49]
1, 2- dihydroxy-anthraquinone**	MeCN	–1.29	–1.08	0.21	4.6	[49]
5, 8- dihydroxy-naphthoquinone**	MeCN	–0.98	–0.91	0.07	2.1	[49]

†Potentials are reported as V vs. SCE. Potentials recorded in MeCN were converted to SCE using Ref. [80].
*Undergoes Kolbe-Schmidt reaction with CO_2 as a decomposition pathway.
**Features intramolecular hydrogen-bonding interactions.
[a]potentials reported in units of volts.
[b]Calculated using approach reported in panel using reported reduction potentials under N_2 and CO_2 atmosphere.

A correlation exists between CO_2 binding affinity of a carrier and its reduction potential. For quinones tested in DMF, Dubois and coworkers observed a linear relationship between the second reduction potential, $E_{1/2(\mathrm{Q_{RA}/Q_{DA}})}$, and the logarithm of the binding coefficient of the dianion, $\log(K_{\mathrm{CO_2(DA)}})$.[66] Figure 2 (left) shows $\log(K_{\mathrm{CO_2(DA)}})$ vs. $E_{1/2(\mathrm{Q_{RA}/Q_{DA}})}$ for various quinones in DMF, DMSO, and MeCN solvents (data from Table 2). Intra-molecular interactions and side reactions with CO_2 disrupt the linear relationship in Figure 2, left. Ogura and coworkers note that quinones featuring intramolecular hydrogen-bonding interactions (indicated by ** in Table 2) display significantly lower CO_2 binding capabilities.[63] Additionally, several quinones have been observed to decompose via Kolbe-Schmitt[81,82] reactions if C–H bonds are present α to the quinone carbonyl groups.[63,66,67,83–85] The side reactivity of these quinones may lead to inaccurate measurements of $K_{\mathrm{CO_2(DA)}}$. If the quinones featuring hydrogen-bonding interactions or Kolbe-Schmidt decomposition are removed from the plot (Figure 2, left), the linear trend becomes more apparent (Figure 2, right). The data in Figure 2 were collected in polar aprotic solvents; the effects of protic or non-polar solvents (as well as cation effects from the supporting salt) may affect this observed linear trend.

2.2 Transition Metal Complexes

Transition metals also have the potential to serve as CO_2 redox carriers by forming a new σ bond between the metal and the electrophilic carbon of CO_2.[83,86] The strength of CO_2 binding (i.e., CO_2 binding coefficient) tends to trend with nucleophilicity. For example, in 1978, Evans et al. reported that CO_2 binding by metal carbonyl anions and empirical nucleophilicities correlated with the reaction rates.[87]

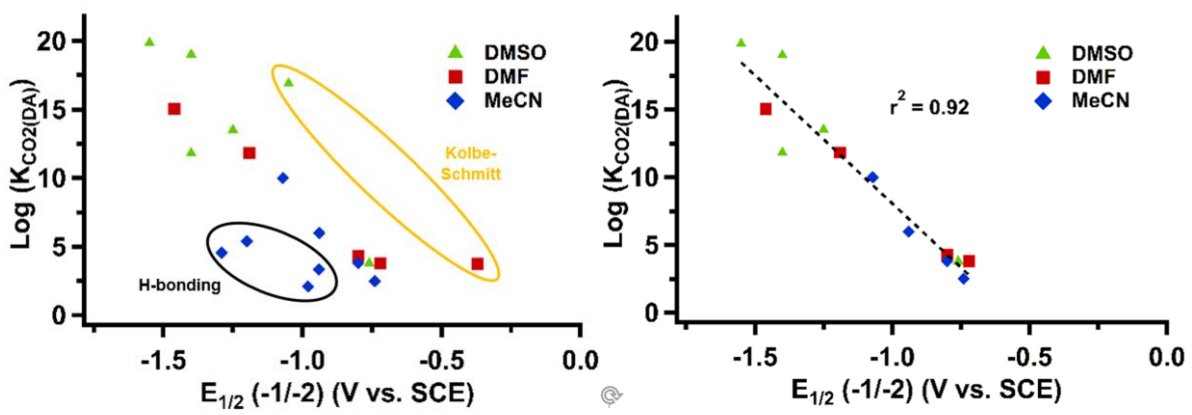

Figure 2: Plots showing trend between $\log(K_{CO_2(DA)})$ and $E_{1/2(Q_{RA}/Q_{DA})}$ (shown as $E_{1/2}$(-1/-2)) for various quinones reported in DMSO (green triangles), DMF (red squares), or MeCN (blue diamonds). Left figure includes quinones that feature intramolecular hydrogen-bonding interactions (circled in black) as well as quinones observed to undergo Kolbe-Schmitt decomposition pathways in the presence of CO_2 (circled in orange). Figure on the right shows that a strong linear correlation exists when the circled quinones with secondary effects or decomposition are removed.

A trend between the CO_2 binding affinity and reduction potential has also been observed for transition metal complexes. The stability of the metal-carboxylate adducts, which are formed upon CO_2 binding, correlates with the M(II/I) reduction potentials.[83,86–89] In transition metal complexes reported to-date, those with reduction potentials negative of -1.90 V vs. $Fc^{+/0}$ exhibit irreversible CO_2 binding, while those with reduction potentials positive of -1.7 V vs. $Fc^{+/0}$ do not react directly with CO_2. Thus, there is only a narrow window in which reversible CO_2 binding is likely to occur, as shown in Figure 3 (left). Due to this limited window, very few measurements on reversible CO_2 binding constants have been made on transition metal complexes; of note is a series Ni(I) and Co(I) tetra-aza macrocyclic complexes described by Lewis and co-workers.[83] A plot of the binding affinity, $\log(K_{CO_2(I)})$, with the reduction potential, $E_{1/2(I/II))}$, results in a linear free energy relationship that correlates more reducing metal centers with stronger, reversible CO_2 binding (Figure 3, left). A similar relationship has been observed in a series of related macrocyclic cobalt complexes.[84]

However, even within this limited data set, other factors that contribute to CO_2 binding are evident that can break this correlation. For instance, the presence of two individual conformers of Me_6[14]-4,11-diene chelate highlighted the importance of flexibility and sterics on CO_2 binding affinities.[83] Although the Co complexes with the Me_6[14]-4,11-diene ligand in the *d*,*l* and *meso*

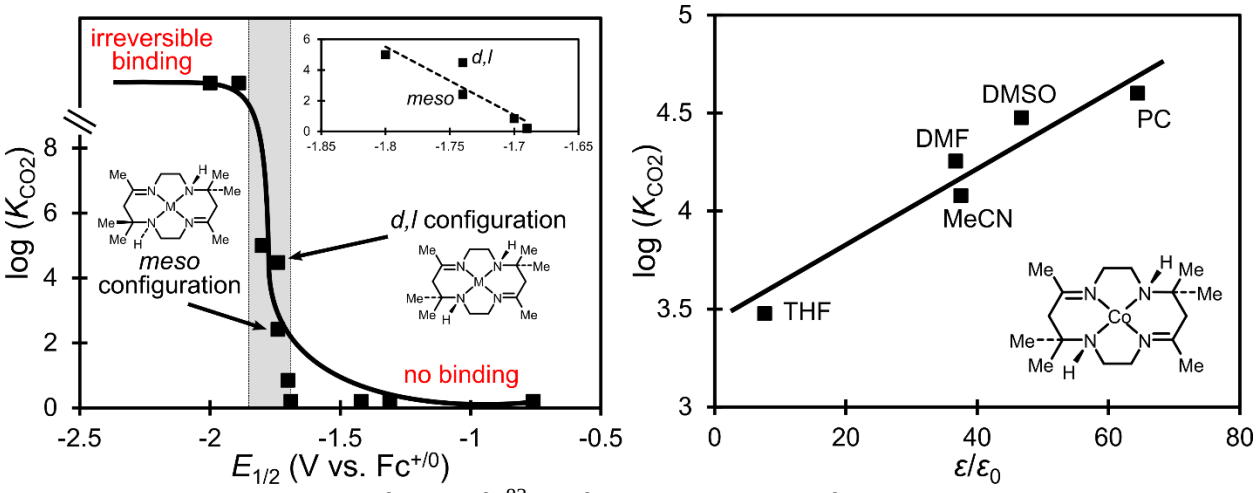

Figure 3. All data are taken from ref. [83]. Left: A relationship of CO_2 binding constants (log *K*) against M(II/I) reduction potentials of different ML complexes; M = Co, Ni. The measurements were obtained in DMSO solution and reported M(II/I) potentials are referred to the ferrocenium/ferrocene ($Fc^{+/0}$) redox couple. An irreversible binding was observed for complexes with reduction potentials more negative than –1.90 V; the binding constants for complexes with potentials more positive than –1.70 V were too low to be measured. Right: A relationship of CO_2 binding constants (log *K*) against dielectric constants ($\varepsilon/\varepsilon_0$) of the used solvent. The measurements were obtained in propylene carbonate, DMSO, DMF, MeCN, and THF.

configurations have identical reduction potentials, the *d, l* has a CO_2 binding constant that is nearly two orders of magnitude larger (*cf.* Figure 3, left) The inhibited binding from the *meso* isomer is likely due to steric factors that impact CO_2-binding.

At the same time, improved CO_2 adduct stabilization for these metal macrocycles may be due to increased hydrogen bonding interactions between the amine hydrogens and the CO_2 oxygen atoms in the *d,l* configuration. Thus, secondary interactions could be useful in the design of new generations of both metal-based and organic carriers. For instance, a number of solvent and electrolyte effects on CO_2 binding to metals are documented,[83] including: *(i)* stabilization of reactants/products in different solvents as the effect of solvent polarity, *(ii)* coordination of a solvent molecule as an axial ligand in the ML complexes, *(iii)* degree of solvation of alkali ions or electrolyte cations, *(iv)* hydrogen bonding interactions, and *(v)* CO_2 solubility. Figure 3 (right) shows a trend between $\log(K_{CO_2(I)})$ and solvent dielectric constants ($\varepsilon/\varepsilon_0$, given as a measure of solvent polarities). A positive correlation is observed, which may be a result of higher stabilization of CO_2 adducts (metal carboxylates) in more polar solvents and/or increased CO_2 solubility.

The presence of ion-pairing may complicate the understanding of solvent effects on CO_2 binding. CO_2 binding affinity has been shown to improve with the assistance of the acidic

partners, such as alkali cations (M^+).[88] A concerted attack of Co(I) on the electrophilic carbon of CO_2 and M^+ interaction with the basic oxygen of CO_2 was observed for bimetallic Co(salen)M complexes.[88,90] Therefore, the extent of solvation of the alkali ions or electrolyte cations in the solution may significantly influence the measured $\log(K_{CO_2(I)})$. As an example, Li^+ ions greatly increase the binding affinity in comparison to, e.g., tetrabutylammonium cations that have the less localized negative charge density.[83,90] Lastly, the effect of Li^+ cations on CO_2 stabilization is more dramatic in THF than in DMSO. This is probably due to a better solvation of Li^+ in DMSO, making the cations less accessible for CO_2 stabilization.

2.3 Design Implications for Stable Carriers

O_2 Stability

O_2 stability of reduced quinones requires reduction potentials positive of the $O_2/O_2^{\bullet-}$ couple.[60,68,70,72,91] Very reducing redox carriers (with reduction potentials negative of this couple) can be oxidized by O_2, to produce superoxide ($O_2^{\bullet-}$) and regenerate the resting-state carrier (Scheme 1, equation I). A cleavage of the C–C bond between the carbonyl groups was observed in the reaction of alpha-diketones (including 1,2-quinones) in air-saturated solution under electrochemical conditions.[62] This decomposition mechanism was attributed to a fast radical coupling of $O_2^{\bullet-}$ and the diketone (quinone) anion radical simultaneously present in a solution, producing the corresponding dicarboxylate species. However, more negative (cathodic) reduction potentials of redox carriers also results in increased CO_2 affinity,[63,66,67,83–85] causing more potent CO_2 carriers to also be more sensitive to O_2. Accordingly, the $E_{1/2(Q_{RA}/Q_{DA})}$ vs. $\log(K_{CO_2(DA)})$ plots shown in Figure 2 reveal that none of the quinones are reduced at potentials less negative than the $O_2/O_2^{\bullet-}$ potential while maintaining appreciable binding constants ($\log(K_{CO_2(DA)}) > 4$). This direct correlation between desired and undesired reactivities requires more detailed consideration of chemical property correlations to design redox carrier-based eCCC systems.

To develop carriers selective for CO_2 binding in the oxygenated atmosphere, they must bind CO_2 at more positive potentials without sacrificing the desirable nucleophilicity. This goal could potentially be achieved by attaching additional auxiliary substituents to include non-covalent interactions for CO_2 binding at its nucleophilic oxygen atoms, e.g., through electrostatics or hydrogen bonding.[63,83,92] This approach can be used for both organic and transition metal complexes. Some of the quinones possessing proton donors (e.g., hydroxyl groups) have been

synthesized.[61] However, the hydroxyl groups in the semiquinones reacted rapidly with molecular oxygen to form hydroperoxide anion radicals – which can further release superoxides – so other CO_2 stabilization might be required.[61]

H_2O Stability

As described above, redox carriers with more cathodic potentials will increase the nucleophilicity of the redox carrier, which leads to an increase in $\log(K_{CO_2})$. However, more cathodic potentials also correlates with Brönsted basicity with quinones[93–95] and transition metals.[96] The positive correlation between $\log(K_{CO_2})$ and pK_b is a challenge to the design of stable carriers, as sufficiently basic carriers may deprotonate H_2O instead of capturing CO_2. From the very limited kinetic data reported for quinone CO_2 reactivity, protonation of the reduced quinone species is kinetically favored over CO_2 binding.[66,75,78] Protonation of anthraquinone has been observed to be twice as fast as CO_2 binding in DMSO.[78] Careful matching of solvent and quinone pK_a and preclusion of acidic proton sources are necessary to prevent kinetic inhibition of eCCC due to protonation.

Although Brönsted basicity is an important parameter to consider for redox carriers, capture can still be performed with an R^{n-} that is more basic than OH^-. In these cases, it is expected that R^{n-} will deprotonate water to generate OH^-, which will then react with CO_2 to form bicarbonate or carbonate. The change in basicity of R/R^{n-} effectively changes the pH of the solution to capture and release CO_2 instead of binding CO_2 directly. These pH swing systems have been described in more detail in recent reviews.[97,98]

Other Effects on Stability

Carriers can be deactivated by the irreversible binding of the CO_2 molecule. This mechanism was observed for some metal-based carriers with highly negative M(II/I) reduction potentials[83] as well as for several quinone molecules that possess *ortho*- or *para*- hydrogens relative to the quinone carbonyl groups.[60,66] In these cases, the Kolbe-Schmidt carboxylation reaction is viable,[99] rendering an adduct that does not allow the CO_2 release. A prominent example of this class of compounds is the inactivation of *p*-benzoquinone after few CO_2 capture/release cycles providing 2,5-dihydroxybenzoic acid.[75]

3. Molecular Engineering of Redox Carriers

Investigation of trends observed in prior work has shown that the key properties for redox carriers - nucleophilicity, basicity, and reduction potentials - are correlated. Generally, increased nucleophilicity is expected to result in greater affinity for CO_2; however, this usually comes with a more negative reduction potential and increased pK_a due to linear free energy relationships (LFER), presenting challenges in optimizing all three properties. A more detailed consideration of chemical property correlations to find characteristics that break these linear free energy relationships is required to effectively design redox carrier molecules for eCCC systems.

Molecular engineering is the practice of modifying the structure of a parent molecule (substituent/ligand environments) to tune its molecular properties, as an optimization task, and has been successfully applied to various families of functional molecules or molecular catalysts.[100–104] Similar to the drug design industry, the role of theory in the molecular design workflow is unitary: it offers trends or insights to guide experimental work (which is much more time- and resource-consuming), meriting low-cost and rapid iteration in accessing a larger chemical space and examining a pool of potential candidates. However, since the accurate prediction of redox potential and binding energies requires free energy calculation at chemical accuracy, the choice of theoretical model is sensitive and multiple realistic aspects may need to be included.

In the following subsections we will discuss the theoretical methods, from computational methods to realistic modeling techniques, for calculating molecular properties and free energetics at chemical accuracy. We will also give a discussion on the inverse design strategies enabled by recent developments in semi-empirical methods, global optimization algorithms, data science and machine learning models.

3.1 Redox Carrier Design with Theoretical Methods

Molecular association in a solution can be viewed as a multi-step process (Figure 4) that consists of: *(i)* change in geometry from the equilibrium structures of the free reactants to the geometry of the product, *(ii)* electronic structure reorganization associated with the formation of new chemical bonds or strong intermolecular interactions, and *(iii)* change in the solvation environment as the two solvation spheres begin to interact and eventually merge. Besides the electronic structure methods, the correct description in computations thus demands a robust

protocol for evaluation of free energies of the equilibrium and transition-state structures of the species involved.

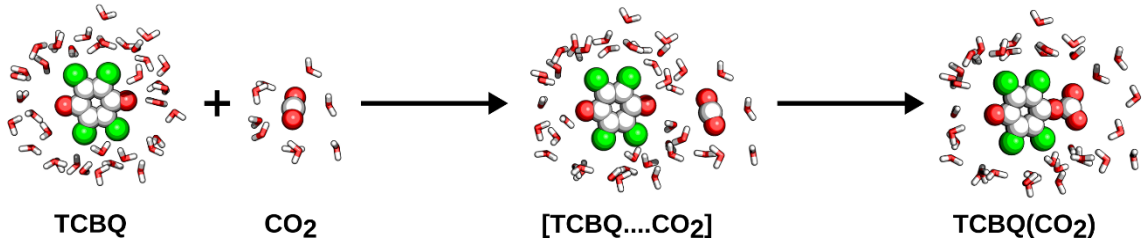

Figure 4. The CO_2 binding in aqueous solution by a prototypical tetrachloro-*p*-benzoquinone (TCBQ) carrier. Within the association, the free reagents (*left*) approach each other to form a 'pre-reaction' bimolecular complex (*middle*). This complex is mainly stabilized by the interactions with the neighboring solvent molecules, making an accurate description of the change in solvent configurational entropy a critical factor for the precision of quantum chemical calculations. The driving force for the association is the formation of a stable molecular entity (*right*), which is regularly accompanied by a significant change in the geometries of the interacting species (e.g., bending of the CO_2 molecule) and electronic structure adjustment as the new chemical bonds are formed.

Sampling of the molecular conformational space

In the real reaction system, the molecules exist as ensembles of different conformations surrounded by different solvent configurations and under the influence of non-uniform external fields. Since the macroscopic observables are essentially thermodynamic ensemble averages, each accessible configuration contributes to the ensemble. Capturing such a tremendous number of degrees of freedom is impractical, but including one or a few of them makes the model more realistic and closer to the physical reality.

According to the Eyring equation, molecules can move across barriers of ~20 kcal/mol on the timescale of minutes at room temperature, and all isomers within ca. 3 kcal/mol could have a significant population. Sampling the huge and complex conformational space with chemical accuracy is therefore an algorithmic challenge for its sheer size. Cheminformatics methods are perhaps the most common and affordable choices for the purpose, which include machine learning models fitted to experimental crystal structures or scripting heuristic rules to build the geometry 'fragment by fragment' according to local connectivity.[105] The knowledge-based algorithms enable the generation of putative global minimum conformer on a personal computer in milliseconds, but the *a priori* geometric constraint also excludes some parts of the conformational

space. Another class of easily affordable methods is the stochastic or systematic torsion scan using molecular mechanics (MM) force field.[106,107] Although more grounded physically, they rely on the proper parametrization of the force field. As a result, the PES may still be far from chemical accuracy, especially in the regions where noncovalent interactions dominate. To describe the energy landscape more accurately, one needs to employ QM methods with an efficient potential energy surface sampling (owing to a much higher computational cost of the local optimization steps). Ensembles generated at a lower level of theory (MM or semiempirical QM) with a higher energy cutoff could serve as decent samples, including those from systematic or stochastic torsion scan, simulated annealing, high-*T* molecular dynamics trajectory, meta-dynamics simulation etc.[108–112]

Modeling of the solvent environment and electrochemical conditions

The interaction between the solvent molecules and the solute is known to affect the energetics of chemical reactions, and the relative stability of the low-energy conformers.[113] Accordingly, the fully explicit treatment of the solvent would be ideal for capturing the specific interatomic interactions. However, since the weak interactions vanish beyond ~4 Å, the explicit QM treatment of only the inner-shell solvent molecules (i.e., microsolvation approach) is a natural approximation to the problem. Including several explicit solvent molecules allows the interaction between solvent and carrier to be studied explicitly, and some intermediate structure that must be stabilized by solvent can be thereby recovered.[114] Such a molecular cluster is notorious for a flat potential energy surface, and a more sophisticated sampling technique is needed. Several algorithms have been adapted to treat the microsolvation model, including particle swarm optimization, genetic algorithm, and basin hopping.[115–117] In terms of energetics, microsolvation models can help to reduce the mean unsigned error of solvation free energy to less than ca. 1.5 kcal/mol; if a proper number of explicit water molecules is adopted.[118] Note that this solvation free energy is dependent on the number of explicit waters, since diverse solvated molecules have different molecular volume and charge distribution that requires altered number of explicit solvent molecules to mimic best the geometry of the solvation complex in a real solution. Even if a decent number of solvent molecules is chosen, the geometry from microsolvation model would still be different from the real solvation environment due to the absence of outer shell solvent molecules that affect the orientation and arrangement of the inner shell solvents. A recent study

showed that the microsolvation model can treat different classes of molecules consistently and reproduce the experimental values only after including more than 20 explicit water molecules,.[119]

Except for the inconsistent performance over molecules of different kinds (dipole, charge state, solvent-accessible area), the microsolvation model also fails to capture the configurational entropy of solvent molecules in a real solution, which is essentially a common drawback of all quantum chemical (QC) calculations based on static models, where the entropy comes only from a single Hessian. To capture the free energy change of the reaction system in solution, in this context, specifically CO_2 binding/release, one-electron reduction/oxidation, and protonation/deprotonation, the statistical mechanical methods outperform "static" methods. Two major approaches to free energy calculation are free energy perturbation (FEP) and thermodynamic integration (TI).[120] In FEP, the system is perturbed along the reaction coordinate, and the total free energy is expressed by summing the successive intermediate steps. In TI, the generalized force is averaged over the sampled configurational space. Due to the statistical nature of FEP and TI, sufficient sampling is required, and the samples can be from Monte Carlo simulation or molecular dynamics trajectory.[121,122] Umbrella sampling can be incorporated to further improve the sampling of the hindered regions in the configurational space.[123] Combined with QM/MM, statistical mechanical methods can treat hundreds if not thousands of explicit water molecules routinely, reproducing experimental energetics of deprotonation and zwitterion dissociation of biomolecules in realistic water solvation, and provide rich chemical insight into the reaction process.[124,125]

At the electrochemical interface, the local environment becomes much more complex. In addition to the carrier molecule and the surrounding solvent molecules, there would be a solid-state electrode, electrolyte forming a double electric layer, and the non-uniform electric field throughout the region. Endeavors have been made to model this kind of an interface at an atomic scale; one of the most popular is the computational hydrogen electrode (CHE) model which converts slab-in-vacuum energetics into corresponding potential values via a linear relationship between reaction free energy and electrode potential.[126] The CHE model has been applied to a wide range of electrocatalytic systems and demonstrated to qualitatively agree with experimental trends; however, it only holds for the systems with coupled proton-electron transfer and cannot account for polarization of the adsorbate at the charged electrode surface. A more theoretical sound treatment is the grand canonical DFT model which connects the system of study to a

reservoir of electrons and allow the number of electrons in the system to vary, so as to model constant-potential chemistries. This can be achieved by charging the system with fractional numbers of electrons, combined with the linearized Poisson-Boltzmann equation for continuum behaviour, to avoid a spurious excess charge and provides much more realistic description of an electric double layer. Such a model has been successfully applied to reveal potential-dependent reaction energetics of CO_2 electroreduction[127] and quantitatively reproduced the adsorption configuration switching of adsorbate on electrode surface at different applied potentials.[128] Although in eCCC no explicit electrochemical conversion of CO_2 is involved, the adsorption behavior and CO_2 binding capacity of a carrier at the electrode could be different as that in the bulk solution, which can represent an extra dimension for optimization.

Another factor in designing or simulating a new carrier is the stability of the molecular structure. In addition to the structure that has substituents with intrinsic instability such as acid chlorides, anhydrides, cyclopentadienes, aziridines, enamines, hemiaminals, enol ethers, cyclobutadiene, cycloheptatriene etc.,[129] some moieties, for example, alpha bromide or iodide (good leaving group), alpha ester and carbonyl (subject to hydrolysis), may appear stable in gas phase simulation but destabilize in protic solvent when the carrier is reduced to an anion or binds a CO_2. Capturing carrier stability thus requires introduction of a sufficient number of explicit solvent molecules and sample beyond the chemical space of interest. Molecular dynamics or meta-dynamics simulation would provide an information on stability by tracing the connectivity along the trajectory, but routinely applying a stability check on every candidate molecule is computational demanding. Therefore, the chemical space must be cautiously defined before the production run; otherwise, a series of molecules that are seemingly practical but unstable under reaction conditions may be generated.

Energetics of the CO_2 binding

Bond-breaking/forming process itself is highly sensitive to the level of theory since the change in bonding is accompanied by a change in the charge localization in the bound/unbound states, charge transfer from one molecule to a binding region, a significant change in the dispersion in going from the free reactants to the product and increasing the static (non-dynamical) correlation. All of these effects are highly problematic for, e.g., the conventional treatment at the density functional theory (DFT) level, since the method neglects the long-range correlation.[130] Some of

the shortcomings may be alleviated by resigning on the kinetic description of the process and focusing only on the thermodynamic (equilibrium) binding. Then, the equilibrium constant of the reaction can be obtained from the free energy difference between the reactant and the product.

For electron donor-acceptor type CO_2 physisorption, in which CO_2 acts as a Lewis acid and the CO_2-philic center as a Lewis base, hydrogen bonding interactions exhibit importance in binding. As an example, a relatively strong interaction was observed between CO_2 and purine molecule (~23 kJ/mol at the CCSD(T)/CBS level), as depicted in Figure 5A.[131] The preferred in-plane binding mode is controlled by the donation of the electron density from nitrogen atom to an electrophilic carbon of the CO_2 group, and the weak hydrogen bond is stabilizing the resulting complex. In Figure 5B, the π-π interaction between CO_2 and the aromatic ring is illustrated. This interaction is another significant contribution to CO_2 binding, which was documented, e.g., in ref. [132], and postulated to be crucial for effectively tuning the uptake efficiency by various metal-organic frameworks (MOFs) or zeolite materials designed for CO_2 adsorption and separation. At last, a different binding pattern was uncovered by Ruiz-Lopez and co-workers, showing the dual role of CO_2 as both Lewis acid and Lewis base when interacting with some carbonyl compounds.[133] A cooperative carbonyl-CO_2 π-π* interaction (Figure 5C) was demonstrated to have comparable interaction energy as the conventional binding.

Regarding the computational methods, the correlation energy was demonstrated to play a critical role for accurate energetics, with dispersion forces accounting for ca. 40 % of the total interaction.[131] Therefore, the post-HF methods were often employed to study interactions of CO_2 with many organic molecules, such as *N*-containing heterocycles[131] and polyheterocycles,[134] amines,[135] organic solvents,[136] aromatic molecules,[132] carbonyl groups,[133,137–139] and other small organic molecules.[140]

Although the DFT methods were revealed to behave unreliably in the prediction of the stability of complexes in Figure 5C (as compared to the CCSD(T)/DZ level of theory),[133] the DFT methods are quite accurate for the weak intermolecular interactions in general, as documented in many benchmark articles.[141–151] Their outcomes should be well applicable also for CO_2 binding equilibrium, especially when combined with the additional dispersion correction methods (e.g., Grimme's D3 empirical dispersion correction[152]). Then, the DFT methods tend to recover up to ca. 90 % of the correlation energy and closely approach the CCSD(T)/CBS limit.

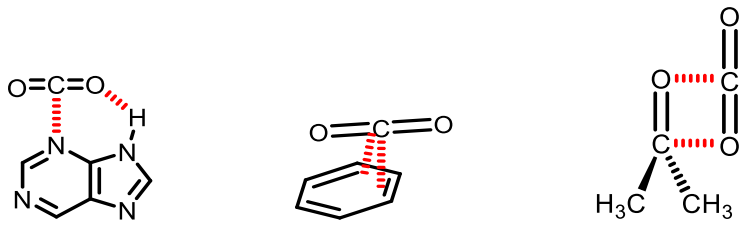

A B C

Figure 5. The main intermolecular interactions involved in the CO_2 physisorption. *A*. The electron donor-acceptor interaction is accompanied by the stabilizing hydrogen-bonding between the oxygen atom of CO_2 and an amine group of purine. *B*. The π-π interaction may become dominant in the aromatic systems. *C*. The dual electron donor-acceptor character of CO_2 is pronounced in its interaction with carbonyl groups.

Further complications might arise when CO_2 is covalently bonded to the (redox) carrier. In this case, the formation of various reaction intermediates can occur, following the initial CO_2 uptake. Their potential interconversion and/or decomposition make the computational treatment difficult, due to the potential energy surface possibly varying dramatically depending on the solvation model (*vide supra*). As an example, there seems to be a clear consensus that amine functionalities bind CO_2 with a direct/indirect participation of the solvent molecules, which also assist in the stabilization of formed intermediates. Inconsistencies in the theoretical models thus mostly originate in the improper modeling of the solvent environment, leading to many contrasting results on the CO_2 binding mechanism. Still, theoretical calculations are important to understanding correlations between CO_2 binding energies and various substituents effects, basicities or nucleophilicities of the CO_2-binding centers, or their influence in the CO_2 stabilization *via* hydrogen-bonding.

As far as the redox eCCC carriers are concerned, the number of computational studies is relatively limited and only exceptionally they extend the standard QM (DFT) with the implicit solvation model approach. On the other hand, the reliability of the methods is often enhanced by their correlation or direct connection with the experiments. A few examples, which include the reaction mechanism for the CO_2 capture by 4,4'-bipyridine (bipy)[72] and *N*-methyl-4,4'-bipyridine (Mebipy)[71], were investigated using DFT (B3LYP and M062X) with the implicit solvation model (IEFPCM or PCM). The computations revealed that a stable adduct is formed between the radical anion of bipy or Mebipy and the CO_2 molecule, with the ΔG_0 = –43.9 kJ/mol or –59 kJ/mol; supporting the results from the CV experiments. The release of the CO_2 molecule was

accomplished by re-oxidation of the adduct, yielding a zwitterionic intermediate susceptible to decarboxylation.

In ref. [68], benzyl disulfide-benzyl thiolate electrochemical cycle was studied computationally at the DFT (B3LYP) level, estimating the binding energy of CO_2 to benzyl thiolate of ca. –66 kJ/mol. A significant electron density localized at the S-C bond of the thiolate and carbon of the CO_2 molecule suggests that upon oxidation, the destabilization should lead to the rapid CO_2 release. Similarly, based on the DFT results from ref. [153], benzyl telluride and benzyl selenide were proposed as potential eCCC agents, as they should have a better peak-to-peak separation between the CO_2 capture and CO_2 release potentials.

Finally, better energetics with the G3MP2//B3LYP composite method with the CPCM solvation model were obtained to explain the different reactivities of *p*-benzoquinone (BQ) and tetrafluoro-*p*-benzoquinone (TFBQ) toward CO_2 capture.[77] BQ was shown to capture CO_2 after the first reduction in the semiquinone state (ECEC mechanism), while TFBQ was proposed to react with CO_2 only after the full (two-electron) reduction was accomplished (EEC mechanism). The lower reactivity of the TFBQ semiquinone was explained based on the lower nucleophilicity of the quinone oxygens due to the electron-withdrawing fluorine atoms. Also, the calculations revealed that TFBQ binds CO_2 at the oxygen atom, forming the carbonate product (favored by ~ 88 kJ/mol over the carboxylate), while the BQ prefers carboxylate by ~ 10 kJ/mol. However, a faster rate toward carbonate formation should circumvent the carboxylate product, which was also validated by the experimental infrared absorption spectroscopy.[154]

CO_2 binding has also been heavily studied in various organic diamines (such as hydrazine, piperazine, etc.), carbonaceous materials, metal/covalent organic frameworks (MOFs/COFs), ultrathin membranes, organic polymers, zeolites, and others, which further complicate the discussion. Many of these systems were reviewed quite recently, with focus on both experimental and theoretical evaluation of the CO_2 interactions, and the interested reader should be referred to relevant articles and references therein (see, e.g., refs. [155–157]).

3.2 Inverse Design of Redox Carriers

Computational High Throughput Screening

An alternative to the bottom-up rational design (based on understanding of the molecular system and substituent effects) is the top-down inverse design methods that start with a desired

property before defining the chemical space. One inverse design approach is the computational high throughput screening or high throughput virtual screening. Assuming there is no prior knowledge about the chemistry or structure-property relationship, the search starts blindly from an expansive library of different kinds of molecules, and multiple filtering processes are gone through to eliminate the unfit molecules, finally reaching a small pool of promising candidates with outstanding properties (Figure 6). Such practice has been applied to *in silico* drug design by the pharmaceutical industry for decades. Empowered by the huge and growing quantity of molecules stored in open databases,[133] researchers can filter through entries to prepare a library of molecules with the help of cheminformatics tools such as OpenBabel,[158] RDKit,[159] and Indigo.[160] The notable databases include ChemSpider,[161] ChEMBL,[162] PubChem,[163] ZINC,[164] and eMolecules,[165] with each specializing in different aspects like bioactivity, physical properties, and commercial availability.

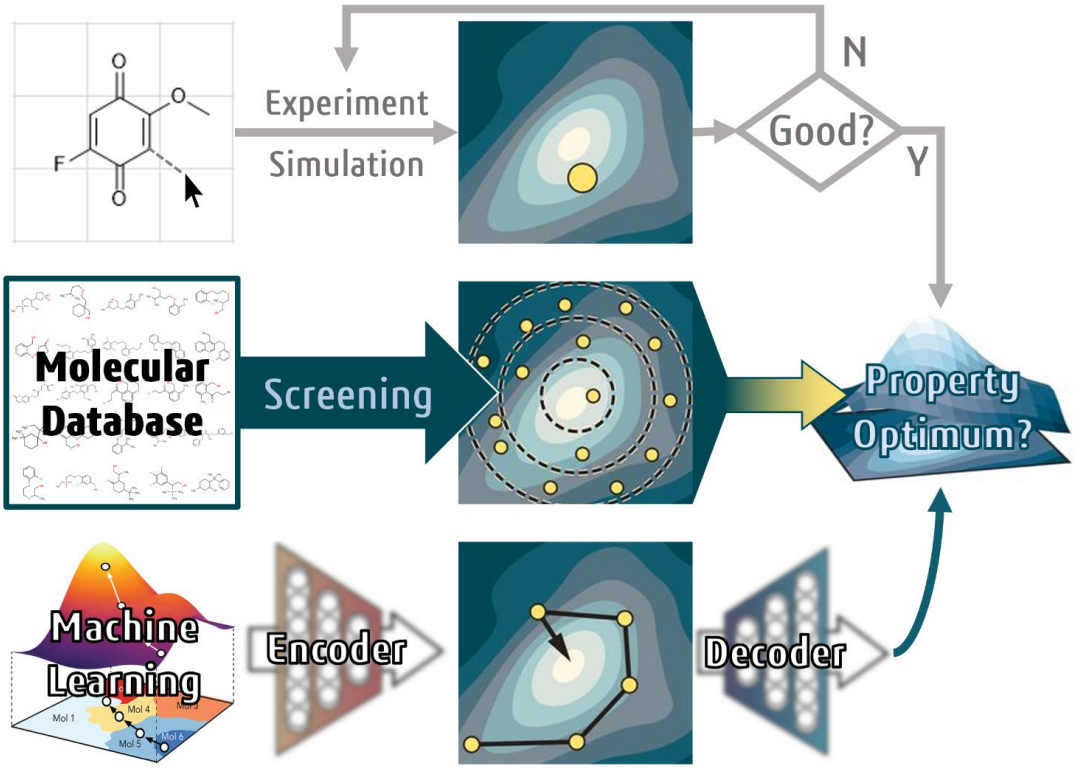

Figure 6. Comparison of the general molecular design workflow via three different strategies: direct design (upper row), inverse design by computational high throughput screening (middle row), and inverse design with generative machine learning model (lower row). Adapted from reference[129,166].

Based on the prepared library of molecules, property descriptors can be constructed to "score" each candidate. Standard techniques include fingerprinting, substructure matching, surface matching to check similarities against a known active molecule or substrate. QSAR models, clustering and partitioning, can also be readily applied to the filtering process using multiple structures as input.[167]

The techniques mentioned above can achieve extremely fast screening speeds; however, as the library is rendered to a smaller size, their performance worsens due to loss of physical and chemical information in these oversimplified representations. In such cases, switching back to more "physical" model can help recover some properties and insights. Molecular mechanics methods, despite successful application to large systems in the last few decades,[168] is outperformed by recently developed efficient quantum chemical methods. The linear-scaling semiempirical method MOZYME-PMn,[169] tight-binding method GFNn-xTB,[170] and revised low-cost density functional method B97-3c[171] can all routinely deal with system of hundreds of atoms on a single processor while providing quantum mechanically meaningful results. Although their accuracy may be off by a few kcal/mol compared to advanced *ab initio* methods, they are capable of cutting down the library to a much more tractable size for advanced QM treatment. It is worth noting that, in 2019, Jensen *et al.* performed high throughput virtual screening through a chemical space of 200 billion molecules in search of energy storage carrier with PM3 and GFN2-xTB,[172] demonstrating the sheer efficiency of semiempirical methods in virtual screening.

Generative Machine Learning Models

Although computational high-throughput screening can greatly expand the investigated chemical space from the experience and intuition of a chemist to all known compounds ever synthesized by the whole community, it is still a small and uneven sampling subset of the complete chemical space. This is where one must go beyond the limit of current synthetic/commercial accessibility and resort to generative machine learning (ML) models. A schematic for the general workflow of inverse molecular design with ML is shown in Figure 6 The molecules are mapped by an encoder into a vector search space for ML where a certain descriptor is maximized or minimized, and then the vectors are converted back to the human-readable molecular format by a decoder. Generating molecular structures that are outside the box but within chemical sense is the major challenge in inverse design with ML, because the ML

models need a search space with well-defined metric and compact embedding of molecular features to ensure that the algorithms and optimizations are efficient and that the outputs are meaningful. Generative tasks are extremely sensitive to the representation of molecular structures, and whether a proper representation is adopted could make or break.[166]

For predictive tasks, the molecular representations that only cover information of local environments would be sufficient, such as bag-of-bonds[173] which summarizes pairwise bonding entities in a molecule, and fingerprint[174] which counts the number of occurrences of different chemical fragments in a molecule. However, they are not suitable for a generative model, which relies heavily on the invertibility of the representation, i.e., the capability to robustly convert into or back from a molecular structure that makes chemical sense. This has something to do with the different nature of the two tasks: a specific property usually depends on a local region near the active site or whether a certain kind of substituent is present, so a minimal representation that can include those would be enough and efficient; but to generate new structures, one needs to establish a robust mapping between points in the vectorized search space to the real-world molecules; otherwise the optimization is likely to lead to a nonsense vector that stands for nothing at all.

The XYZ coordinates or Z-matrix, which are standard representations for ab initio calculations, straightforwardly describe the atomic positions but are not suitable for ML models since they either could not offer a description of the intrinsic structural features or are difficult to be convert into consistent matrix representations due to undefined length/size. If the desired search space is relatively local, e.g., all 3-substituted quinones, one can naturally define a parent system where the substituent positions are predefined and then one-hot encode the ligands' type and position into an $M \times N$-D vector where the M is the size of ligand pool and N is the number of possible sites. Such representation allows exploration of chemical space of size $\sim M^N$ (permutations included), which can then be feed to global optimization algorithms such as genetic algorithm to locate the extrema of a specific property.[172,175] However, such discretized and fixed-dimensionality encoding entirely relies on chemical knowledge of the system, therefore confining the search space in the predefined space.

Focusing on the atomic connectivity in a molecule leads to molecular graphs where only information of atom types (as nodes) and connectivity (as edges) are retained, e.g., SMILES[176] and SMARTS.[177] Such representations "translate" the geometry into a 1D string text by a grammar based on empirical bonding principles in a molecule, which offers a higher level of abstraction

while maintaining readability. However, the NLP-like search space suffers from discretization, which makes the model not directly suitable for generative ML tasks, because simple vectorization of SMILES would lead to generation of nonsense strings that are rejected by their strict grammar. One solution then is to train a variational autoencoder (VAE) framework to encode the discrete strings into a point in continuous latent space, which is readily available for interpolation, optimization, and random exploration.[129] Within the latent space, one can implement local or global optimization algorithms combined with predictive models to evaluate the property descriptor at each point and optimize toward a maximized property. After the optimization, the points in latent space with descriptors above a certain criterion can be converted back into the original representation format with another decoder model. It requires teaching the encoder and decoder models to read and write in SMILES grammar, and such additional training and validation need to be repeated for each different class of molecules. Generative Adversarial Networks (GAN) can do a similar job by co-training a discriminator model and a fake generator model to judge whether a string-based representation is legal or not. GAN, when combined with the latent space approach, has been reported to work well in both random generation and target biased generation,[178] but it requires a larger volume of pre-training data and more hyperparameter tuning.[179]

Another solution is to devise a more robust string-based representation that translates even entirely random strings to practical molecular structures. Aspuru-Guzik *et al*. recently proposed Self-Referencing Embedded Strings (SELFIES) to be a 100% robust string-based representation that covers the complete chemical space of molecules through a self-referencing syntax.[180] SELFIES can be directly used in designing workflow without further adaptation or encoder/decoder training. Coulomb matrix is emerging as another promising molecular representation. It is essentially a sparse matrix that contains pairwise Coulombic forces between atoms, which entails richer physical information, and is principally suitable for tasks related to electronic properties.[181,182]

Image-based representation is another growing field that is powered by advances in computer vision and image recognition in the last decade. In 2018, Zhavoronkov et al. constructed a 3D image representation of molecular structure based on wave transform and convolutional neural network. In 2019, Vogiatzis *et al.* proposed a persistence image (PI) representation based on the

persistent homology mathematics, which provides a topological representation and has been applied to identify 44 new CO_2 binders based on an active learning model.[183]

Another challenge is the scarcity of data. Even for properties that are relatively inexpensive and easy to determine, for example, pK_a, the size of the database is usually no more than a few thousand for a certain class of molecules. Other properties, such as the CO_2 binding constant or redox potential in a specific solvent, may be costlier or more demanding, leading to an even more severe lack of data. Automation does not help much since ML needs data points of different molecules using the same setting, and the rate-limiting factor of the whole workflow is the commercial availability or synthesis of molecules, while most automation set-ups aim to optimize experimental parameters such as concentration, temperature, pressure, and choice of solvents. Data augmentation techniques, such as symmetry-based expansion or neural networks making use of non-uniqueness of SMILES,[184] helps improving prediction-oriented models but does not make chemical space richer for generative tasks. A promising approach is the jointly training over a combined dataset of experimental and *ab initio* result to achieve data enrichment and to explore expanded chemical space.[185]

A universal or generalized ML model for exploration of chemical space may not exist at all; even if there can be one, it may not work well. The difficulty originates in the intrinsic discontinuity of chemical space of practical molecules – they are deep wells scattering over the potential energy surface separated by unstable structures – and the knowledge to avoid the impractical regions must be provided by either *ad hoc* prior with chemical insights (encoding grammar, formatting, predefined chemical environment and fragments, ligand pool) or sufficiently large and reliable experimental dataset (which is not available); otherwise a myriad of disordered atomic clusters may dominate the set. Such sparse nature of chemical space also makes hyperparameter tuning (learning rate, batch size) and convergence difficult, especially on a diverse dataset. The tradeoff between complete sampling of chemical space and producing practical molecules are somewhat contradictory. Despite the unsatisfactory transferability, generative ML models are still the best possible tools at the moment to locally explore the chemical space of a specific class of chemicals to optimize the desired property.

4. Conclusion and Outlook

Electrochemical CO_2 capture and concentration has significantly higher theoretical energetic efficiencies compared to thermal methods. Although the field is still in its infancy, the

few reported systems using redox carriers have thermodynamic efficiencies that rival or exceed current state-of-the-art amine-based capture systems.[186–188] However, practical implementation requires improvements to the performance, stability, and efficiency of the redox carriers. The current systems perform at <10% of the theoretical efficiency, but these values could be improved by modifying the redox carrier CO_2 binding constant (K_{CO2}) and reduction potential ($E_{1/2}$). However, the reduction potential ($E_{1/2}$) is also a critical property towards redox carrier sensitivity towards O_2, while undesirable reactivity with water is dictated by its pK_a. In this tutorial review, we discuss how these values are correlated through scaling relationships, leading to undesirable trade-offs for the respective properties. We describe the use of experimental and computational methods to pursue design strategies for redox carriers that deviate from these scaling relationships leading to more optimal properties.

Box/Panel 1 Experimentally Measuring CO_2 Binding Constants

Determination of K_{CO_2} for the active and resting states of redox carriers can be determined utilizing numerous methods. The use of electrochemical methods, however, are unique to redox carriers. Large carrier CO_2 binding constants (K_{CO_2} > 100) can be measured using the observed shift in the reduction potential recorded in the presence ($E'_{1/2}$) and absence ($E_{1/2}$) of a known concentration of CO_2 by applying equation 7.[83,89]

$$E'_{1/2} = E_{1/2} + \frac{RT}{nF}\ln\left(K_{CO_2}\right) + q\frac{RT}{nF}\ln\left[CO_2\right] \quad \textbf{7}$$

Where R is the universal gas constant (8.314 J mol^{-1} K^{-1}), T is absolute temperature (K), F is the Faraday constant (96485 C mol^{-1}), and n is the number of electrons being passed in the redox event. The number of CO_2 molecules that are bound during the chemical step is represented by the term q (typically, q = 1 or 2, and can be determined via other spectroscopic or voltametric techniques).[66,67,189] For carriers where K_{CO_2} < 100, the assumption that $K_{CO_2}[CO_2]$ >> 1 (which is used to derive equation 7) is no longer valid, and equation 8 must be used instead, where q is assumed to be 1.[83]

$$E'_{1/2} = E_{1/2} + \frac{RT}{nF}\ln\left(K_{CO_2}[CO_2] + 1\right) \quad \textbf{8}$$

This approach can be highly beneficial, as it does not require isolation of the active state carrier, which can often be unstable or difficult to isolate cleanly. Furthermore, the approach can be

utilized for carriers spanning a large range of K_{CO_2} (K_{CO_2} values ranging between <10 to >10^{15} have been reported using this method)[63,66,67,83]. Values of K_{CO_2} for redox-carriers can be also be determined using more common spectroscopic or physical techniques, depending on the magnitude of K_{CO_2} and solubility of the carrier. These techniques include, but are not limited to: NMR and electronic absorption spectroscopy, gravimetry, and gas uptake experiments.[66,67,84,85]

References:

(1) International Energy Agency. *Net Zero by 2050*; Paris, 2021.

(2) Gabrielli, P.; Gazzani, M.; Mazzotti, M. The Role of Carbon Capture and Utilization, Carbon Capture and Storage, and Biomass to Enable a Net-Zero-CO2 Emissions Chemical Industry. *Ind. Eng. Chem. Res.* **2020**, *59* (15), 7033–7045. https://doi.org/10.1021/ACS.IECR.9B06579.

(3) Bui, M.; Adjiman, C. S.; Bardow, A.; Anthony, E. J.; Boston, A.; Brown, S.; Fennell, P. S.; Fuss, S.; Galindo, A.; Hackett, L. A.; et al. Carbon Capture and Storage (CCS): The Way Forward. *Energy Environ. Sci.* **2018**, *11*, 1176. https://doi.org/10.1039/c7ee02342a.

(4) Wang, M.; Lawal, A.; Stephenson, P.; Sidders, J.; Ramshaw, C. Post-Combustion CO2 Capture with Chemical Absorption: A State-of-the-Art Review. *Chem. Eng. Res. Des.* **2011**, *89* (9), 1609–1624. https://doi.org/10.1016/J.CHERD.2010.11.005.

(5) Wang, X.; Song, C. Carbon Capture From Flue Gas and the Atmosphere: A Perspective. *Front. Energy Res.* **2020**, *0*, 265. https://doi.org/10.3389/FENRG.2020.560849.

(6) Fasihi, M.; Efimova, O.; Breyer, C. Techno-Economic Assessment of CO2 Direct Air Capture Plants. *J. Clean. Prod.* **2019**, *224*, 957–980. https://doi.org/10.1016/j.jclepro.2019.03.086.

(7) Socolow, R.; Desmond, M.; Aines, R.; Blackstock, J.; Bolland, O.; Kaarsberg, T.; Lewis, N.; Mazzotti, M.; Pfeffer, A.; Sawyer, K.; et al. Direct Air Capture of CO2 with Chemicals: A Technology Assessment for the APS Panel on Public Affairs. *Am. Phys. Soc.* **2011**.

(8) International Association of Oil & Gas Producers. Global CCUS projects: Overview of existing and planned CCUS facilities.

(9) Wilberforce, T.; Baroutaji, A.; Soudan, B.; Al-Alami, A. H.; Olabi, A. G. Outlook of Carbon Capture Technology and Challenges. *Sci. Total Environ.* **2019**, *657*, 56–72. https://doi.org/10.1016/J.SCITOTENV.2018.11.424.

(10) Leung, D. Y. C.; Caramanna, G.; Maroto-Valer, M. M. An Overview of Current Status of Carbon Dioxide Capture and Storage Technologies. *Renew. Sustain. Energy Rev.* **2014**, *39*, 426–443. https://doi.org/10.1016/J.RSER.2014.07.093.

(11) Sanz-Pérez, E. S.; Murdock, C. R.; Didas, S. A.; Jones, C. W. Direct Capture of CO2 from

Ambient Air. *Chem. Rev.* **2016**, *116* (19), 11840–11876. https://doi.org/10.1021/acs.chemrev.6b00173.

(12) Wilcox, J.; Psarras, P. C.; Liguori, S. Assessment of Reasonable Opportunities for Direct Air Capture. *Environ. Res. Lett.* **2017**, *12* (6), 065001. https://doi.org/10.1088/1748-9326/AA6DE5.

(13) Heldebrant, D.; Jiang, Y.; Zheng, R.; Barpaga, D.; Freeman, C.; Koech, P. K.; Malhotra, D.; Whyatt, G.; Zwoster, A. Performance and Cost Predictions of 2-EEMPA, and Future Opportunities for Water-Lean Post-Combustion Capture Solvents. *Proc. 15th Greenh. Gas Control Technol. Conf. 15-18 March 2021* **2021**. https://doi.org/10.2139/SSRN.3813876.

(14) Krekel, D.; Samsun, R. C.; Peters, R.; Stolten, D. The Separation of CO2 from Ambient Air – A Techno-Economic Assessment. *Appl. Energy* **2018**, *218*, 361–381. https://doi.org/10.1016/J.APENERGY.2018.02.144.

(15) Liu, Y.; Deng, S.; Zhao, R.; He, J.; Zhao, L. Energy-Saving Pathway Exploration of CCS Integrated with Solar Energy: A Review of Innovative Concepts. *Renew. Sustain. Energy Rev.* **2017**, *77*, 652–669. https://doi.org/10.1016/J.RSER.2017.04.031.

(16) Jiang, L.; Wang, R. Q.; Gonzalez-Diaz, A.; Smallbone, A.; Lamidi, R. O.; Roskilly, A. P. Comparative Analysis on Temperature Swing Adsorption Cycle for Carbon Capture by Using Internal Heat/Mass Recovery. *Appl. Therm. Eng.* **2020**, *169*, 114973. https://doi.org/10.1016/J.APPLTHERMALENG.2020.114973.

(17) Noël, T.; Cao, Y.; Laudadio, G. The Fundamentals Behind the Use of Flow Reactors in Electrochemistry. *Acc. Chem. Res.* **2019**, *52* (10), 2858–2869. https://doi.org/10.1021/ACS.ACCOUNTS.9B00412.

(18) Yan, M.; Kawamata, Y.; Baran, P. S. Synthetic Organic Electrochemical Methods Since 2000: On the Verge of a Renaissance. *Chem. Rev.* **2017**, *117* (21), 13230–13319. https://doi.org/10.1021/ACS.CHEMREV.7B00397.

(19) Meyer, T. H.; Choi, I.; Tian, C.; Ackermann, L. Powering the Future: How Can Electrochemistry Make a Difference in Organic Synthesis? *Chem* **2020**, *6* (10), 2484–2496. https://doi.org/10.1016/J.CHEMPR.2020.08.025.

(20) Tanbouza, N.; Ollevier, T.; Lam, K. Bridging Lab and Industry with Flow Electrochemistry. *iScience* **2020**, *23* (11), 101720. https://doi.org/10.1016/J.ISCI.2020.101720.

(21) Gulaboski, R. Electrochemistry in the Twenty-First Century—Future Trends and Perspectives. *J. Solid State Electrochem.* **2020**, *24* (9), 2081. https://doi.org/10.1007/S10008-020-04550-0.

(22) Huebscher, R. G.; Babinsky, A. D. Electrochemical Concentration and Separation of Carbon Dioxide for Advanced Life Support Systems - Carbonation Cell System. *SAE Tech. Pap.* **1969**, No. 690640, 2164–2170. https://doi.org/10.4271/690640.

(23) Dell'Osso, L.; Ruder, J. M.; Winnick, J. Mixed-Gas Adsorption and Vacuum Desorption of Carbon Dioxide on Molecular Sieve. Bed Performance and Data Analysis. *Ind. Eng. Chem. Process Des. Dev.* **2002**, *8* (4), 477–482. https://doi.org/10.1021/I260032A007.

(24) Schbert, F. H.; Marshall, R. D.; Hallick, T. M.; Woods, R. R.; Marshall, R. D.; Hallick, T. M.; Woods, R. R. *One-Man Electrochemical Air Revitalization System Evaluation*; Cleveland, OH, 1976.

(25) Eisaman, M. D.; Schwartz, D. E.; Amic, S.; Larner, D.; Zesch, J.; Torres, F.; Littau, K. Energy-Efficient Electrochemical CO2 Capture from the Atmosphere. *TechConnect Briefs* **2009**, No. 2009, 175–178.

(26) Winnick, J.; Marshall, R. D.; Schubert, F. H. An Electrochemical Device for Carbon Dioxide Concentration, i. System Design and Performance. *Ind. Eng. Chem. Process Des. Dev.* **1974**, *13* (1), 59–63. https://doi.org/10.1021/i260049a011.

(27) Kang, M. P.; Winnick, J. Concentration of Carbon Dioxide by a High-Temperature Electrochemical Membrane Cell. *J. Appl. Electrochem.* **1985**, *15* (3), 431–439. https://doi.org/10.1007/BF00615996.

(28) Srinivas, G.; Krungleviciute, V.; Guo, Z. X.; Yildirim, T. Exceptional CO2 Capture in a Hierarchically Porous Carbon with Simultaneous High Surface Area and Pore Volume. *Energy Environ. Sci.* **2014**, *7* (1), 335–342. https://doi.org/10.1039/c3ee42918k.

(29) Jiang, H. L.; Liu, B.; Lan, Y. Q.; Kuratani, K.; Akita, T.; Shioyama, H.; Zong, F.; Xu, Q. From Metal-Organic Framework to Nanoporous Carbon: Toward a Very High Surface Area and Hydrogen Uptake. *J. Am. Chem. Soc.* **2011**, *133* (31), 11854–11857. https://doi.org/10.1021/JA203184K/SUPPL_FILE/JA203184K_SI_001.PDF.

(30) Wang, Q.; Xia, W.; Guo, W.; An, L.; Xia, D.; Zou, R. Functional Zeolitic-Imidazolate-Framework-Templated Porous Carbon Materials for CO2 Capture and Enhanced Capacitors. *Chem. – An Asian J.* **2013**, *8* (8), 1879–1885. https://doi.org/10.1002/ASIA.201300147.

(31) Aijaz, A.; Fujiwara, N.; Xu, Q. From Metal-Organic Framework to Nitrogen-Decorated Nanoporous Carbons: High CO2 Uptake and Efficient Catalytic Oxygen Reduction. *J. Am. Chem. Soc.* **2014**, *136* (19), 6790–6793. https://doi.org/10.1021/JA5003907/SUPPL_FILE/JA5003907_SI_001.PDF.

(32) Wang, M.; Hariharan, S.; Shaw, R. A.; Hatton, T. A. Energetics of Electrochemically Mediated Amine Regeneration Process for Flue Gas CO2 Capture. *Int. J. Greenh. Gas Control* **2019**, *82*, 48–58. https://doi.org/https://doi.org/10.1016/j.ijggc.2018.12.028.

(33) Wang, M.; Herzog, H. J.; Hatton, T. A. CO2 Capture Using Electrochemically Mediated Amine Regeneration. *Ind. Eng. Chem. Res.* **2020**, *59* (15), 7087–7096. https://doi.org/10.1021/ACS.IECR.9B05307.

(34) Liu, G. X.; Yu, Y. S.; Hong, Y. T.; Zhang, Z. X.; Wei, J. J.; Wang, G. G. X. Identifying Electrochemical Effects in a Thermal–Electrochemical Co-Driven System for CO2 Capture. *Phys. Chem. Chem. Phys.* **2017**, *19* (20), 13230–13244. https://doi.org/10.1039/C7CP01035D.

(35) Stern, M. C.; Simeon, F.; Herzog, H.; Hatton, T. A. Post-Combustion Carbon Dioxide Capture Using Electrochemically Mediated Amine Regeneration. https://doi.org/10.1039/c3ee41165f.

(36) Stern, M. C.; Alan Hatton, T. Bench-Scale Demonstration of CO2 Capture with Electrochemically-Mediated Amine Regeneration. *RSC Adv.* **2014**, *4* (12), 5906–5914. https://doi.org/10.1039/c3ra46774k.

(37) Eltayeb, A. O.; Stern, M. C.; Herzog, H.; Hatton, T. A. Energetics of Electrochemically-Mediated Amine Regeneration. *Energy Procedia* **2014**, *63*, 595–604. https://doi.org/10.1016/J.EGYPRO.2014.11.064.

(38) Ye, W.; Huang, J.; Lin, J.; Zhang, X.; Shen, J.; Luis, P.; Van Der Bruggen, B. Environmental Evaluation of Bipolar Membrane Electrodialysis for NaOH Production from Wastewater: Conditioning NaOH as a CO2 Absorbent. *Sep. Purif. Technol.* **2015**, *144*, 206–214. https://doi.org/10.1016/J.SEPPUR.2015.02.031.

(39) Jin, S.; Wu, M.; Gordon, R. G.; Aziz, M. J.; Kwabi, D. G. PH Swing Cycle for CO2 Capture Electrochemically Driven through Proton-Coupled Electron Transfer. *Energy Environ. Sci.* **2020**, *13* (10), 3706–3722. https://doi.org/10.1039/D0EE01834A.

(40) Rahimi, M.; Catalini, G.; Hariharan, S.; Wang, M.; Puccini, M.; Hatton, T. A. Carbon Dioxide Capture Using an Electrochemically Driven Proton Concentration Process. *Cell Reports Phys. Sci.* **2020**, *1* (4), 100033. https://doi.org/10.1016/J.XCRP.2020.100033.

(41) Huang, C.; Liu, C.; Wu, K.; Yue, H.; Tang, S.; Lu, H.; Liang, B. CO_2 Capture from Flue Gas Using an Electrochemically Reversible Hydroquinone/Quinone Solution. *Energy & Fuels* **2019**, *33* (4), 3380–3389. https://doi.org/10.1021/acs.energyfuels.8b04419.

(42) Watkins, J. D.; Siefert, N. S.; Zhou, X.; Myers, C. R.; Kitchin, J. R.; Hopkinson, D. P.; Nulwala, H. B. Redox-Mediated Separation of Carbon Dioxide from Flue Gas. *Energy and Fuels* **2015**, *29* (11), 7508–7515. https://doi.org/10.1021/ACS.ENERGYFUELS.5B01807.

(43) Kwabi, D. G.; Aziz, M. J.; John, H.; Paulson, A. PH Swing Cycle for CO2 Capture Electrochemically Driven through Proton-Coupled Electron Transfer. **2019**. https://doi.org/10.26434/CHEMRXIV.7853414.V1.

(44) Xie, H.; Wu, Y.; Liu, T.; Wang, F.; Chen, B.; Liang, B. Low-Energy-Consumption Electrochemical CO2 Capture Driven by Biomimetic Phenazine Derivatives Redox Medium. *Appl. Energy* **2020**, *259*, 114119. https://doi.org/10.1016/J.APENERGY.2019.114119.

(45) Xie, H.; Jiang, W.; Liu, T.; Wu, Y.; Wang, Y.; Chen, B.; Niu, D.; Liang, B. Low-Energy Electrochemical Carbon Dioxide Capture Based on a Biological Redox Proton Carrier. *Cell Reports Phys. Sci.* **2020**, *1* (5), 100046. https://doi.org/10.1016/J.XCRP.2020.100046.

(46) Lackner, K. S. The Thermodynamics of Direct Air Capture of Carbon Dioxide. *Energy* **2013**, *50* (1), 38–46. https://doi.org/10.1016/j.energy.2012.09.012.

(47) Li, L.; Wong-Ng, W.; Huang, K.; P. Cook, L. *Materials and Processes for CO2 Capture, Conversion, and Sequestration*, 1st ed.; John Wiley & Sons: Hoboken, NJ, 2018.

(48) Jiang, Y.; Ling, J.; Xiao, P.; He, Y.; Zhao, Q.; Chu, Z.; Liu, Y.; Li, Z.; Webley, P. A. Simultaneous Biogas Purification and CO2 Capture by Vacuum Swing Adsorption Using Zeolite NaUSY. *Chem. Eng. J.* **2018**, *334*, 2593–2602.

https://doi.org/10.1016/J.CEJ.2017.11.090.

(49) Herron, S. E.; Zoelle, A.; Summers, W. M. *Cost of Capturing CO2 from Industrial Sources*; Pittsburgh, PA, 2014.

(50) Allen, J. G.; MacNaughton, P.; Cedeno-Laurent, J. G.; Cao, X.; Flanigan, S.; Vallarino, J.; Rueda, F.; Donnelly-McLay, D.; Spengler, J. D. Airplane Pilot Flight Performance on 21 Maneuvers in a Flight Simulator under Varying Carbon Dioxide Concentrations. *J. Expo. Sci. Environ. Epidemiol. 2018 294* **2018**, *29* (4), 457–468. https://doi.org/10.1038/s41370-018-0055-8.

(51) Stern, M. C.; Simeon, F.; Hammer, T.; Landes, H.; Herzog, H. J.; Hatton, T. A. Electrochemically Mediated Separation for Carbon Capture. *Energy Procedia* **2011**, *4*, 860–867. https://doi.org/10.1016/j.egypro.2011.01.130.

(52) Clarke, L. E.; Leonard, M. E.; Hatton, T. A.; Brushett, F. R. Thermodynamic Modeling of CO2 Separation Systems with Soluble, Redox-Active Capture Species. *ChemRxiv* **2021**. https://doi.org/10.33774/chemrxiv-2021-2dqk6.

(53) Voskian, S.; Hatton, T. A. Faradaic Electro-Swing Reactive Adsorption for CO 2 Capture. *Energy Environ. Sci.* **2019**, *12*, 3530–3547. https://doi.org/10.1039/c9ee02412c.

(54) Liu, Y.; Ye, H. Z.; Diederichsen, K. M.; Van Voorhis, T.; Hatton, T. A. Electrochemically Mediated Carbon Dioxide Separation with Quinone Chemistry in Salt-Concentrated Aqueous Media. *Nat. Commun. 2020 111* **2020**, *11* (1), 1–11. https://doi.org/10.1038/s41467-020-16150-7.

(55) Voskian, S.; Hatton, T. A. Faradaic Electro-Swing Reactive Adsorption for CO2 Capture. *Energy Environ. Sci* **2019**, *12*, 3530. https://doi.org/10.1039/c9ee02412c.

(56) Shaw, R. A.; Hatton, T. A. Electrochemical CO2 Capture Thermodynamics. *Int. J. Greenh. Gas Control* **2020**, *95* (June 2019), 102878. https://doi.org/10.1016/j.ijggc.2019.102878.

(57) Scovazzo, P.; Poshusta, J.; DuBois, D.; Koval, C.; Noble, R. Electrochemical Separation and Concentration of <1% Carbon Dioxide from Nitrogen. *J. Electrochem. Soc.* **2003**, *150* (5), D91. https://doi.org/10.1149/1.1566962.

(58) Fuller, T. F.; John N. Harb. *Electrochemical Engineering*; John Wiley & Sons, Inc.: Hoboken, 2018.

(59) Wilcox, J.; Rochana, P.; Kirchofer, A.; Glatz, G.; He, J. Revisiting Film Theory to Consider Approaches for Enhanced Solvent-Process Design for Carbon Capture. **2014**. https://doi.org/10.1039/c4ee00001c.

(60) Rheinhardt, J. H.; Singh, P.; Tarakeshwar, P.; Buttry, D. A. Electrochemical Capture and Release of Carbon Dioxide. *ACS Energy Lett.* **2017**, *2* (2), 454–461. https://doi.org/10.1021/acsenergylett.6b00608.

(61) Jeziorek, D.; Ossowski, T.; Liwo, A.; Dyl, D.; Nowacka, M.; Woz, W. Theoretical and Electrochemical Study of the Mechanism of Anthraquinone-Mediated One-Electron Reduction of Oxygen: The Involvement of Adducts of Dioxygen Species to

Anthraquinones. *J. Chem. Soc., Perkin Trans* **1997**, *2*, 229–236. https://doi.org/10.1039/A605549D.

(62) Boujlel, K.; Simonet, J. On the Electrochemical Reduction of α-Diketones in the Presence of Oxygen. *Tetrahedron Lett.* **1979**, *20* (12), 1063–1066. https://doi.org/10.1016/S0040-4039(01)87192-6.

(63) Nagaoka, T.; Nishii, N.; Fujii, K.; Ogura, K. Mechanisms of Reductive Addition of CO2 to Quinones in Acetonitrile. *J. Electroanal. Chem.* **1992**, *322* (1–2), 383–389. https://doi.org/10.1016/0022-0728(92)80090-Q.

(64) Jain, P. S.; Lal, S. Electrolytic Reduction of Oxygen at Solid Electrodes in Aprotic Solvents-the Superoxide Ion. *Electrochim. Acta* **1982**, *27* (6), 759–763. https://doi.org/10.1016/0013-4686(82)85071-8.

(65) Yu, Q.; Ye, S. In Situ Study of Oxygen Reduction in Dimethyl Sulfoxide (DMSO) Solution: A Fundamental Study for Development of the Lithium-Oxygen Battery. *J. Phys. Chem. C* **2015**, *119* (22), 12236–12250. https://doi.org/10.1021/ACS.JPCC.5B03370.

(66) Dubois, D. L.; Miedaner, A.; Bell, W.; Smart, J. C. Electrochemical Concentration of Carbon Dioxide. In *Electrochemical and Electrocatalytic Reactions of Carbon Dioxide*; Sullivan, B. R., Ed.; Elsevier: Amsterdam, 1993; pp 94–117.

(67) Bell, W. L.; Miedaner, A.; Smart, J. C.; DuBois, D. L. Synthesis and Evaluation of Electroactive CO2 Carriers. *SAE Technical Paper Series*. 1988, pp 1–10.

(68) Singh, P.; Rheinhardt, J. H.; Olson, J. Z.; Tarakeshwar, P.; Mujica, V.; Buttry, D. A. Electrochemical Capture and Release of Carbon Dioxide Using a Disulfide-Thiocarbonate Redox Cycle. *J. Am. Chem. Soc.* **2017**, *139* (3). https://doi.org/10.1021/jacs.6b10806.

(69) Pipes, R.; Bhargav, A.; Manthiram, A. Phenyl Disulfide Additive for Solution-Mediated Carbon Dioxide Utilization in Li–CO2 Batteries. *Adv. Energy Mater.* **2019**, *9* (21), 1900453. https://doi.org/https://doi.org/10.1002/aenm.201900453.

(70) Ishida, H.; Ohba, T.; Yamaguchi, T.; Ohkubo, K. Interaction between CO₂ and Electrochemically Reduced Species of N-Propyl-4,4′-Bipyridinium Cation. *Chem. Lett.* **1994**, *23* (5), 905–908. https://doi.org/10.1246/cl.1994.905.

(71) Singh, P.; Tarakeshwar, P.; Buttry, D. A. Experimental, Simulation, and Computational Study of the Interaction of Reduced Forms of N-Methyl-4,4'-Bipyridinium with CO2. *ChemElectroChem* **2020**, *7* (2), 469–475. https://doi.org/https://doi.org/10.1002/celc.201901884.

(72) Ranjan, R.; Olson, J.; Singh, P.; Lorance, E. D.; Buttry, D. A.; Gould, I. R. Reversible Electrochemical Trapping of Carbon Dioxide Using 4,4′-Bipyridine That Does Not Require Thermal Activation. *J. Phys. Chem. Lett.* **2015**, *6* (24), 4943–4946. https://doi.org/10.1021/acs.jpclett.5b02220.

(73) Guin, P. S.; Das, S.; Mandal, P. C. Electrochemical Reduction of Quinones in Different Media: A Review. *Int. J. Electrochem.* **2011**, *2011*, 1–22. https://doi.org/10.4061/2011/816202.

(74) Simeon, F.; Stern, M. C.; Diederichsen, K. M.; Liu, Y.; Herzog, H. J.; Hatton, A. Electrochemical and Molecular Assessment of Quinones as CO2-Binding Redox Molecules for Carbon Capture. *J. Phys. Chem. C* **2021**, *126* (3), 1389–1399. https://doi.org/10.1021/acs.jpcc.1c09415.

(75) De Sousa Bulhõesw, L. O.; Zara, A. J. The Effect of Carbon Dioxide on the Electroreduction of 1,4-Benzoquinone. *J. Electroanal. Chem. Interfacial Electrochem.* **1988**, *248* (1), 159–165. https://doi.org/10.1016/0022-0728(88)85158-1.

(76) Gupta, N.; Linschitz, H. Hydrogen-Bonding and Protonation Effects in Electrochemistry of Quinones in Aprotic Solvents. *J. Am. Chem. Soc.* **1997**, *119* (27), 6384–6391. https://doi.org/10.1021/JA970028J.

(77) Namazian, M.; Zare, H. R.; Yousofian-Varzaneh, H. Electrochemical Behavior of Tetrafluoro-p-Benzoquinone at the Presence of Carbon Dioxide: Experimental and Theoretical Studies. *Electrochim. Acta* **2016**, *196*, 692–698. https://doi.org/10.1016/J.ELECTACTA.2016.02.159.

(78) Comeau Simpson, T.; Durand, R. R. Reactivity of Carbon Dioxide with Quinones. *Electrochim. Acta* **1990**, *35* (9), 1399–1403. https://doi.org/10.1016/0013-4686(90)85012-C.

(79) Qiao, X.; Li, D.; Cheng, L.; Jin, B. Mechanism of Electrochemical Capture of CO2 via Redox Cycle of Chlorinated 1,4-Naphthoquinone in BMIMBF4: An in-Situ FT-IR Spectroelectrochemical Approach. *J. Electroanal. Chem.* **2019**, *845*, 126–136. https://doi.org/10.1016/j.jelechem.2019.05.057.

(80) Pavlishchuk, V. V; Addison, A. W. Conversion Constants for Redox Potentials Measured versus Different Reference Electrodes in Acetonitrile Solutions at 25°C. *Inorganica Chim. Acta* **2000**, *298* (1), 97–102. https://doi.org/https://doi.org/10.1016/S0020-1693(99)00407-7.

(81) Luo, J.; Preciado, S.; Xie, P.; Larrosa, I. Carboxylation of Phenols with CO2 at Atmospheric Pressure. *Chem. – A Eur. J.* **2016**, *22* (20), 6798–6802. https://doi.org/10.1002/CHEM.201601114.

(82) Hudnall, P. M. Hydroquinone. *Ullmann's Encycl. Ind. Chem.* **2000**. https://doi.org/10.1002/14356007.A13_499.

(83) Schmidt, M. H.; Miskelly, G. M.; Lewis, N. S. Effects of Redox Potential, Steric Configuration, Solvent, and Alkali Metal Cations on the Binding of Carbon Dioxide to Cobalt(I) and Nickel(I) Macrocycles. *J. Am. Chem. Soc.* **1990**, *112* (9), 3420–3426. https://doi.org/10.1021/ja00165a027.

(84) Creutz, C.; Schwarz, H. A.; Wishart, J. F.; Fujita, E.; Sutin, N. Thermodynamics and Kinetics of Carbon Dioxide Binding to Two Stereoisomers of a Cobalt(I) Macrocycle in Aqueous Solution. *J. Am. Chem. Soc.* **2002**, *113* (9), 3361–3371. https://doi.org/10.1021/JA00009A022.

(85) Creutz, C. Carbon Dioxide Binding To Transition-Metal Centers. In *Electrochemical and Electrocatalytic Reactions of Carbon Dioxide*; Sullivan, B. R., Ed.; Elsevier: Amsterdam,

1993; pp 19–67. https://doi.org/10.1016/B978-0-444-88316-2.50006-1.

(86) Schneider, J.; Jia, H.; Muckerman, J. T.; Fujita, E. Thermodynamics and Kinetics of CO2, CO, and H+ Binding to the Metal Centre of CO2reductioncatalysts. *Chem. Soc. Rev.* **2012**, *41* (6), 2036–2051. https://doi.org/10.1039/C1CS15278E.

(87) Evans, G. O.; Walter, W. F.; Mills, D. R.; Streit, C. A. Reactions of Carbon Dioxide with Metal Carbonyl Anions. *J. Organomet. Chem.* **1978**, *144* (2), C34–C38. https://doi.org/10.1016/S0022-328X(00)84173-X.

(88) Fachinetti, G.; Floriani, C.; Zanazzi, P. F. Bifunctional Activation of Carbon Dioxide. Synthesis and Structure of a Reversible Carbon Dioxide Carrier. *J. Am. Chem. Soc.* **2002**, *100* (23), 7405–7407. https://doi.org/10.1021/JA00491A045.

(89) Gangi, D. A.; Durand, R. R. Binding of Carbon Dioxide to Cobalt and Nickel Tetra-Aza Macrocycles. *J. CHEM. SOC., CHEM. COMMUN* **1986**, No. 9, 697–699. https://doi.org/10.1039/C39860000697.

(90) Gambarotta, S.; Arena, F.; Floriani, C.; Zanazzi, P. F. Carbon Dioxide Fixation: Bifunctional Complexes Containing Acidic and Basic Sites Working as Reversible Carriers. *J. Am. Chem. Soc.* **1982**, *104* (19), 5082–5092. https://doi.org/10.1021/JA00383A015/SUPPL_FILE/JA00383A015_SI_001.PDF.

(91) Singh, S.; Stechel, E. B.; Buttry, D. A. Transient Modeling of Electrochemically Assisted CO2 Capture and Release. *J. Electroanal. Chem.* **2017**, *799*. https://doi.org/10.1016/j.jelechem.2017.05.045.

(92) Han, C.; Li, H.; Shi, R.; Zhang, T.; Tong, J.; Li, J.; Li, B. Organic Quinones towards Advanced Electrochemical Energy Storage: Recent Advances and Challenges. *J. Mater. Chem. A* **2019**, *7* (41), 23378–23415. https://doi.org/10.1039/C9TA05252F.

(93) Mayr, H.; Ofial, A. R. Do General Nucleophilicity Scales Exist? *J. Phys. Org. Chem.* **2008**, *21* (7–8), 584–595. https://doi.org/10.1002/POC.1325.

(94) Zhu, X. Q.; Wang, C. H.; Liang, H. Scales of Oxidation Potentials, p K a, and BDE of Various Hydroquinones and Catechols in DMSO. *J. Org. Chem.* **2010**, *75* (21), 7240–7257. https://doi.org/10.1021/JO101455M.

(95) Huynh, M. T.; Anson, C. W.; Cavell, A. C.; Stahl, S. S.; Hammes-Schiffer, S. Quinone 1 e − and 2 e − /2 H + Reduction Potentials: Identification and Analysis of Deviations from Systematic Scaling Relationships. **2016**. https://doi.org/10.1021/jacs.6b05797.

(96) Yang, J. Y.; Kerr, T. A.; Wang, X. S.; Barlow, J. M. Reducing CO2 to HCO2- at Mild Potentials: Lessons from Formate Dehydrogenase. *J. Am. Chem. Soc.* **2020**, *142* (46), 19438–19445. https://doi.org/10.1021/JACS.0C07965/SUPPL_FILE/JA0C07965_SI_001.PDF.

(97) Sharifian, R.; Wagterveld, R. M.; Digdaya, I. A.; Xiang, C.; Vermaas, D. A. Electrochemical Carbon Dioxide Capture to Close the Carbon Cycle. *Energy Environ. Sci.* **2021**, *14* (2), 781–814. https://doi.org/10.1039/D0EE03382K.

(98) Renfrew, S. E.; Starr, D. E.; Strasser, P. Electrochemical Approaches toward CO2 Capture

and Concentration. *ACS Catal.* **2020**, *10* (21), 13058–13074. https://doi.org/10.1021/acscatal.0c03639.

(99) Lindsey, A. S.; Jeskey, H. The Kolbe-Schmitt Reaction. *Chem. Rev.* **2002**, *57* (4), 583–620. https://doi.org/10.1021/CR50016A001.

(100) Ding, Y.; Zhang, C.; Zhang, L.; Zhou, Y.; Yu, G. Molecular Engineering of Organic Electroactive Materials for Redox Flow Batteries. *Chem. Soc. Rev.* **2018**, *47* (1), 69–103. https://doi.org/10.1039/C7CS00569E.

(101) Zhang, X.; Wang, Y.; Gu, M.; Wang, M.; Zhang, Z.; Pan, W.; Jiang, Z.; Zheng, H.; Lucero, M.; Wang, H.; et al. Molecular Engineering of Dispersed Nickel Phthalocyanines on Carbon Nanotubes for Selective CO 2 Reduction. https://doi.org/10.1038/s41560-020-0667-9.

(102) Dickerson, C. E.; Guo, H.; Shin, A. J.; Augenbraun, B. L.; Caram, J. R.; Campbell, W. C.; Alexandrova, A. N. Franck-Condon Tuning of Optical Cycling Centers by Organic Functionalization. *Phys. Rev. Lett.* **2021**, *126* (12), 123002. https://doi.org/10.1103/PHYSREVLETT.126.123002.

(103) Jimenez-Izal, E.; Liu, J. Y.; Alexandrova, A. N. Germanium as Key Dopant to Boost the Catalytic Performance of Small Platinum Clusters for Alkane Dehydrogenation. *J. Catal.* **2019**, *374*, 93–100. https://doi.org/10.1016/J.JCAT.2019.04.034.

(104) Deng, J.; Lin, S. C.; Fuller, J. T.; Zandkarimi, B.; Chen, H. M.; Alexandrova, A. N.; Liu, C. Electrocatalytic Methane Functionalization with D0 Early Transition Metals Under Ambient Conditions. *Angew. Chemie Int. Ed.* **2021**, *60* (51), 26630–26638. https://doi.org/10.1002/ANIE.202107720.

(105) Yoshikawa, N.; Hutchison, G. R. Fast, Efficient Fragment-Based Coordinate Generation for Open Babel. *J. Cheminform.* **2019**, *11* (1), 1–9. https://doi.org/10.1186/S13321-019-0372-5.

(106) Gürsoy, O.; Smieško, M. Searching for Bioactive Conformations of Drug-like Ligands with Current Force Fields: How Good Are We? **2017**, *9*, 29. https://doi.org/10.1186/s13321-017-0216-0.

(107) O'Boyle, N. M.; Vandermeersch, T.; Flynn, C. J.; Maguire, A. R.; Hutchison, G. R. Confab - Systematic Generation of Diverse Low-Energy Conformers. *J. Cheminform.* **2011**, *3* (1), 1–9. https://doi.org/10.1186/1758-2946-3-8.

(108) Smith, G. D.; Jaffe, R. L.; Yoon, D. Y.; Astrup, F. E.; Ogawa, Y.; Ohta, M.; Sakakibara, M.; Matsuura, H.; Harada, I.; Shimanouchi, T.; et al. Conformations of 1,2-Dimethoxyethane in the Gas and Liquid Phases from Molecular Dynamics Simulations. *J. Am. Chem. Soc.* **2002**, *117* (1), 530–531. https://doi.org/10.1021/JA00106A061.

(109) Sun, Y.; Kollman, P. A. Conformational Sampling and Ensemble Generation by Molecular Dynamics Simulations: 18-Crown-6 as a Test Case. *J. Comput. Chem.* **1992**, *13* (1), 33–40. https://doi.org/10.1002/JCC.540130105.

(110) Grimme, S. Exploration of Chemical Compound, Conformer, and Reaction Space with Meta-Dynamics Simulations Based on Tight-Binding Quantum Chemical Calculations. *J.*

Chem. Theory Comput. **2019**, *15* (5), 2847–2862. https://doi.org/10.1021/ACS.JCTC.9B00143.

(111) Jothi, P. R.; Zhang, Y.; Scheifers, J. P.; Park, H.; Fokwa, B. P. T. Molybdenum Diboride Nanoparticles as a Highly Efficient Electrocatalyst for the Hydrogen Evolution Reaction. *Sustain. Energy Fuels* **2017**, *1* (9), 1928–1934. https://doi.org/10.1039/C7SE00397H.

(112) Auffinger, P.; Wipff, G. High Temperature Annealed Molecular Dynamics Simulations as a Tool for Conformational Sampling. Application to the Bicyclic "222" Cryptand. *J. Comput. Chem.* **1990**, *11* (1), 19–31. https://doi.org/10.1002/JCC.540110103.

(113) Li, Y.; Hartke, B. Assessing Solvation Effects on Chemical Reactions with Globally Optimized Solvent Clusters. *ChemPhysChem* **2013**, *14* (12), 2678–2686. https://doi.org/10.1002/CPHC.201300323.

(114) Gupta, M.; Da Silva, E. F.; Svendsen, H. F. Postcombustion CO2 Capture Solvent Characterization Employing the Explicit Solvation Shell Model and Continuum Solvation Models. *J. Phys. Chem. B* **2016**, *120* (34), 9034–9050. https://doi.org/10.1021/ACS.JPCB.6B04049/SUPPL_FILE/JP6B04049_SI_001.PDF.

(115) Zhang, J.; Dolg, M. Global Optimization of Clusters of Rigid Molecules Using the Artificial Bee Colony Algorithm. *Phys. Chem. Chem. Phys.* **2016**, *18* (4), 3003–3010. https://doi.org/10.1039/C5CP06313B.

(116) Alexandrova, A. N. H·(H2O)n Clusters: Microsolvation of the Hydrogen Atom via Molecular Ab Initio Gradient Embedded Genetic Algorithm (GEGA). *J. Phys. Chem. A* **2010**, *114* (48), 12591–12599. https://doi.org/10.1021/JP1092543.

(117) Burnham, C. J.; Petersen, M. K.; Day, T. J. F.; Iyengar, S. S.; Voth, G. A. The Properties of Ion-Water Clusters. II. Solvation Structures of Na+, Cl−, and H+ Clusters as a Function of Temperature. *J. Chem. Phys.* **2006**, *124* (2), 024327. https://doi.org/10.1063/1.2149375.

(118) Sutton, C. C. R.; Franks, G. V.; Da Silva, G. First Principles PKa Calculations on Carboxylic Acids Using the SMD Solvation Model: Effect of Thermodynamic Cycle, Model Chemistry, and Explicit Solvent Molecules. *J. Phys. Chem. B* **2012**, *116* (39), 11999–12006. https://doi.org/10.1021/JP305876R.

(119) Basdogan, Y.; Groenenboom, M. C.; Henderson, E.; De, S.; Rempe, S. B.; Keith, J. A. Machine Learning-Guided Approach for Studying Solvation Environments. *J. Chem. Theory Comput.* **2020**, *16* (1), 633–642. https://doi.org/10.1021/ACS.JCTC.9B00605.

(120) Kästner, J.; Senn, H. M.; Thiel, S.; Otte, N.; Thiel, W. QM/MM Free-Energy Perturbation Compared to Thermodynamic Integration and Umbrella Sampling: Application to an Enzymatic Reaction. *J. Chem. Theory Comput.* **2006**, *2* (2), 452–461. https://doi.org/10.1021/CT050252W.

(121) Alexandrova, A. N.; Jorgensen, W. L. Why Urea Eliminates Ammonia Rather than Hydrolyzes in Aqueous Solution. *J. Phys. Chem. B* **2007**, *111* (4), 720–730. https://doi.org/10.1021/JP066478S.

(122) Shivakumar, D.; Williams, J.; Wu, Y.; Damm, W.; Shelley, J.; Sherman, W. Prediction of Absolute Solvation Free Energies Using Molecular Dynamics Free Energy Perturbation

and the Opls Force Field. *J. Chem. Theory Comput.* **2010**, *6* (5), 1509–1519. https://doi.org/10.1021/CT900587B.

(123) Souaille, M.; Roux, B. Extension to the Weighted Histogram Analysis Method: Combining Umbrella Sampling with Free Energy Calculations. *Comput. Phys. Commun.* **2001**, *135* (1), 40–57. https://doi.org/10.1016/S0010-4655(00)00215-0.

(124) Nelson, J. G.; Peng, Y.; Silverstein, D. W.; Swanson, J. M. J. Multiscale Reactive Molecular Dynamics for Absolute p K a Predictions and Amino Acid Deprotonation. *J. Chem. Theory Comput.* **2014**, *10* (7), 2729–2737. https://doi.org/10.1021/CT500250F.

(125) Alexandrova, A. N.; Jorgensen, W. L. On the Mechanism and Rate of Spontaneous Decomposition of Amino Acids. *J. Phys. Chem. B* **2011**, *115*, 13624–13632. https://doi.org/10.1021/jp2081808.

(126) Nørskov, J. K.; Rossmeisl, J.; Logadottir, A.; Lindqvist, L.; Kitchin, J. R.; Bligaard, T.; Jónsson, H. Origin of the Overpotential for Oxygen Reduction at a Fuel-Cell Cathode. **2004**. https://doi.org/10.1021/jp047349j.

(127) Steinmann, S. N.; Michel, C.; Schwiedernoch, R.; Sautet, P. Impacts of Electrode Potentials and Solvents on the Electroreduction of CO 2 : A Comparison of Theoretical Approaches †. *Phys. Chem. Chem. Phys* **2015**, *17*, 13949. https://doi.org/10.1039/c5cp00946d.

(128) Steinmann, S. N.; Sautet, P. Assessing a First-Principles Model of an Electrochemical Interface by Comparison with Experiment. *J. Phys. Chem. C* **2016**, *120* (10), 5619–5623. https://doi.org/10.1021/ACS.JPCC.6B01938.

(129) Gómez-Bombarelli, R.; Wei, J. N.; Duvenaud, D.; Hernández-Lobato, J. M.; Sánchez-Lengeling, B.; Sheberla, D.; Aguilera-Iparraguirre, J.; Hirzel, T. D.; Adams, R. P.; Aspuru-Guzik, A. Automatic Chemical Design Using a Data-Driven Continuous Representation of Molecules. *ACS Cent. Sci.* **2018**, *4* (2), 268–276. https://doi.org/10.1021/ACSCENTSCI.7B00572.

(130) Mardirossian, N.; Head-Gordon, M. Thirty Years of Density Functional Theory in Computational Chemistry: An Overview and Extensive Assessment of 200 Density Functionals. *Mol. Phys.* **2017**, *115* (19), 2315–2372. https://doi.org/10.1080/00268976.2017.1333644.

(131) Vogiatzis, K. D.; Mavrandonakis, A.; Klopper, W.; Froudakis, G. E. Ab Initio Study of the Interactions between CO2 and N-Containing Organic Heterocycles. *ChemPhysChem* **2009**, *10* (2), 374–383. https://doi.org/10.1002/CPHC.200800583.

(132) Chen, L.; Cao, F.; Sun, H. Ab Initio Study of the π–π Interactions between CO2 and Benzene, Pyridine, and Pyrrole. *Int. J. Quantum Chem.* **2013**, *113* (20), 2261–2266. https://doi.org/10.1002/QUA.24444.

(133) Altarsha, M.; Ingrosso, F.; Ruiz-Lopez, M. F. A New Glimpse into the CO2-Philicity of Carbonyl Compounds. *ChemPhysChem* **2012**, *13* (14), 3397–3403. https://doi.org/10.1002/CPHC.201200135.

(134) Li, S.; Smith, D. G. A.; Patkowski, K. An Accurate Benchmark Description of the

Interactions between Carbon Dioxide and Polyheterocyclic Aromatic Compounds Containing Nitrogen. *Phys. Chem. Chem. Phys.* **2015**, *17* (25), 16560–16574. https://doi.org/10.1039/C5CP02365C.

(135) Jorgensen, K. R.; Cundari, T. R.; Wilson, A. K. Interaction Energies of CO 2·amine Complexes: Effects of Amine Substituents. *J. Phys. Chem. A* **2012**, *116* (42), 10403–10411. https://doi.org/10.1021/JP305347B/.

(136) Zhang, X.; Han, X.; Xu, W. A COMPUTER SIMULATION STUDY ON LEWIS ACID–BASE INTERACTIONS AND COOPERATIVE C-H···O WEAK HYDROGEN BONDING IN VARIOUS CO2 COMPLEXES. *https://doi.org/10.1142/S0219633611006591* **2012**, *10* (4), 483–508. https://doi.org/10.1142/S0219633611006591.

(137) Nelson, M. R.; Borkman, R. F. Ab Initio Calculations on CO2 Binding to Carbonyl Groups. *J. Phys. Chem. A* **1998**, *102* (40), 7860–7863. https://doi.org/10.1021/JP981824U.

(138) San-Fabián, E.; Ingrosso, F.; Lambert, A.; Bernal-Uruchurtu, M. I.; Ruiz-López, M. F. Theoretical Insights on Electron Donor–Acceptor Interactions Involving Carbon Dioxide. *Chem. Phys. Lett.* **2014**, *601*, 98–102. https://doi.org/10.1016/J.CPLETT.2014.03.084.

(139) Dang Cam-Tu, P.; Thi Ngan, V.; Tien Trung, N. General Trends in Structure, Stability and Role of Interactions in the Complexes of Acetone and Thioacetone with Carbon Dioxide and Water. *Chem. Phys.* **2020**, *530*, 110580. https://doi.org/10.1016/J.CHEMPHYS.2019.110580.

(140) Lee, H. M.; Youn, I. S.; Saleh, M.; Lee, J. W.; Kim, K. S. Interactions of CO2 with Various Functional Molecules. *Phys. Chem. Chem. Phys.* **2015**, *17* (16), 10925–10933. https://doi.org/10.1039/C5CP00673B.

(141) Sherrill, C. D. Frontiers in Electronic Structure Theory. *J. Chem. Phys.* **2010**, *132* (11), 110902. https://doi.org/10.1063/1.3369628.

(142) Riley, K. E.; Pitoňák, M.; Jurečka, P.; Hobza, P. Stabilization and Structure Calculations for Noncovalent Interactions in Extended Molecular Systems Based on Wave Function and Density Functional Theories. *Chem. Rev.* **2010**, *110* (9), 5023–5063. https://doi.org/10.1021/CR1000173.

(143) Grimme, S. Density Functional Theory with London Dispersion Corrections. *Wiley Interdiscip. Rev. Comput. Mol. Sci.* **2011**, *1* (2), 211–228. https://doi.org/10.1002/WCMS.30.

(144) Burns, L. A.; Vázquez-Mayagoitia, Á.; Sumpter, B. G.; Sherrill, C. D. Density-Functional Approaches to Noncovalent Interactions: A Comparison of Dispersion Corrections (DFT-D), Exchange-Hole Dipole Moment (XDM) Theory, and Specialized Functionals. *J. Chem. Phys.* **2011**, *134* (8), 084107. https://doi.org/10.1063/1.3545971.

(145) Hohenstein, E. G.; Sherrill, C. D. Wavefunction Methods for Noncovalent Interactions. *Wiley Interdiscip. Rev. Comput. Mol. Sci.* **2012**, *2* (2), 304–326. https://doi.org/10.1002/WCMS.84.

(146) Riley, K. E.; Hobza, P. Noncovalent Interactions in Biochemistry. *Wiley Interdiscip. Rev. Comput. Mol. Sci.* **2011**, *1* (1), 3–17. https://doi.org/10.1002/WCMS.8.

(147) Klimeš, J.; Michaelides, A. Perspective: Advances and Challenges in Treating van Der Waals Dispersion Forces in Density Functional Theory. *J. Chem. Phys.* **2012**, *137* (12), 120901. https://doi.org/10.1063/1.4754130.

(148) Tkatchenko, A.; Tkatchenko, A. Current Understanding of Van Der Waals Effects in Realistic Materials. *Adv. Funct. Mater.* **2015**, *25* (13), 2054–2061. https://doi.org/10.1002/adfm.201403029.

(149) Reilly, A. M.; Tkatchenko, A. Van Der Waals Dispersion Interactions in Molecular Materials: Beyond Pairwise Additivity. *Chem. Sci.* **2015**, *6* (6), 3289–3301. https://doi.org/10.1039/C5SC00410A.

(150) Řezáč, J.; Hobza, P. Benchmark Calculations of Interaction Energies in Noncovalent Complexes and Their Applications. *Chem. Rev.* **2016**, *116* (9), 5038–5071. https://doi.org/10.1021/acs.chemrev.5B00526.

(151) Řezáč, J.; Bím, D.; Gutten, O.; Rulíšek, L. Toward Accurate Conformational Energies of Smaller Peptides and Medium-Sized Macrocycles: MPCONF196 Benchmark Energy Data Set. *J. Chem. Theory Comput.* **2018**, *14* (3), 1254–1266. https://doi.org/10.1021/acs.jctc.7B01074.

(152) Grimme, S.; Antony, J.; Ehrlich, S.; Krieg, H. A Consistent and Accurate Ab Initio Parametrization of Density Functional Dispersion Correction (DFT-D) for the 94 Elements H-Pu. *J. Chem. Phys.* **2010**, *132* (15). https://doi.org/10.1063/1.3382344.

(153) Harris, D.; Bushnell, E. Density Functional Theory Study of the Capture and Release of Carbon Dioxide by Benzyl-Disulfide, -Diselenide, and -Ditelluride. *J. Phys. Chem. A* **2019**, *123* (15), 3383–3388. https://doi.org/10.1021/acs.jpca.9B01862.

(154) Fan, H.; Cheng, L.; Jin, B. Investigation on Electrochemical Capture of CO2 in P-Benzoquinone Solutions by in Situ FT-IR Spectroelectrochemistry. *Electrochim. Acta* **2019**, *324*, 134882. https://doi.org/10.1016/j.electacta.2019.134882.

(155) Tian, Z.; Dai, S.; Jiang, D. en. What Can Molecular Simulation Do for Global Warming? *Wiley Interdiscip. Rev. Comput. Mol. Sci.* **2016**, *6* (2), 173–197. https://doi.org/10.1002/WCMS.1241.

(156) Stowe, H. M.; Hwang, G. S. Fundamental Understanding of CO2 Capture and Regeneration in Aqueous Amines from First-Principles Studies: Recent Progress and Remaining Challenges. *Ind. Eng. Chem. Res.* **2017**, *56* (24), 6887–6899. https://doi.org/10.1021/ACS.IECR.7B00213.

(157) Yang, X.; Rees, R. J.; Conway, W.; Puxty, G.; Yang, Q.; Winkler, D. A. Computational Modeling and Simulation of CO 2 Capture by Aqueous Amines. *Chem. Rev.* **2017**, *117* (14), 9524–9593. https://doi.org/10.1021/acs.chemrev.6b00662.

(158) O'Boyle, N. M.; Banck, M.; James, C. A.; Morley, C.; Vandermeersch, T.; Hutchison, G. R. Open Babel: An Open Chemical Toolbox. *J. Cheminform.* **2011**, *3* (10), 1–14. https://doi.org/10.1186/1758-2946-3-33.

(159) Landrum, G. RDKit: Open-Source Cheminformatics. 2006.

(160) Pavlov, D.; Rybalkin, M.; Karulin, B.; Kozhevnikov, M.; Savelyev, A.; Churinov, A. Indigo: Universal Cheminformatics API. *J. Cheminform.* **2011**, *3* (SUPPL. 1), 1–1. https://doi.org/10.1186/1758-2946-3-S1-P4.

(161) Pence, H. E.; Williams, A. ChemSpider: An Online Chemical Information Resource. *J. Chem. Educ.* **2010**, *87* (11), 1123–1124. https://doi.org/10.1021/ED100697W.

(162) Gaulton, A.; Hersey, A.; Nowotka, M. L.; Patricia Bento, A.; Chambers, J.; Mendez, D.; Mutowo, P.; Atkinson, F.; Bellis, L. J.; Cibrian-Uhalte, E.; et al. The ChEMBL Database in 2017. *Nucleic Acids Res.* **2017**, *45* (D1), D945–D954. https://doi.org/10.1093/NAR/GKW1074.

(163) Kim, S.; Thiessen, P. A.; Bolton, E. E.; Chen, J.; Fu, G.; Gindulyte, A.; Han, L.; He, J.; He, S.; Shoemaker, B. A.; et al. PubChem Substance and Compound Databases. *Nucleic Acids Res.* **2016**, *44* (D1), D1202–D1213. https://doi.org/10.1093/nar/gkv951.

(164) Sterling, T.; Irwin, J. J. ZINC 15 – Ligand Discovery for Everyone. *J. Chem. Inf. Model.* **2015**, *55* (11), 2324–2337. https://doi.org/10.1021/acs.jcim.5B00559.

(165) EMolecules Database.

(166) Sanchez-Lengeling, B.; Aspuru-Guzik, A. Inverse Molecular Design Using Machine Learning: Generative Models for Matter Engineering. *Science (80-.).* **2018**, *361* (6400), 360–365. https://doi.org/10.1126/science.aat2663.

(167) Bajorath, J. Integration of Virtual and High-Throughput Screening. *Nat. Rev. Drug Discov. 2002 111* **2002**, *1* (11), 882–894. https://doi.org/10.1038/nrd941.

(168) Kumari, R.; Kumar, R.; Lynn, A. G-Mmpbsa-A GROMACS Tool for High-Throughput MM-PBSA Calculations. *J. Chem. Inf. Model.* **2014**, *54* (7), 1951–1962. https://doi.org/10.1021/ci500020m.

(169) Sulimov, A.; Kutov, D.; Ilin, I.; Sulimov, V. Quantum-Chemical Quasi-Docking for Molecular Dynamics Calculations. *Nanomaterials* **2022**, *12* (2), 1–13. https://doi.org/10.3390/nano12020274.

(170) Bannwarth, C.; Ehlert, S.; Grimme, S. GFN2-XTB—An Accurate and Broadly Parametrized Self-Consistent Tight-Binding Quantum Chemical Method with Multipole Electrostatics and Density-Dependent Dispersion Contributions. *J. Chem. Theory Comput.* **2019**, *15* (3), 1652–1671. https://doi.org/10.1021/acs.jctc.8b01176.

(171) Brandenburg, J. G.; Bannwarth, C.; Hansen, A.; Grimme, S. B97-3c: A Revised Low-Cost Variant of the B97-D Density Functional Method. *J. Chem. Phys.* **2018**, *148* (6), 064104. https://doi.org/10.1063/1.5012601.

(172) Koerstz, M.; Christensen, A. S.; Mikkelsen, K. V.; Nielsen, M. B.; Jensen, J. H. High Throughput Virtual Screening of 200 Billion Molecular Solar Heat Battery Candidates. *ChemRxiv* **2020**. https://doi.org/10.26434/chemrxiv.8003813.V1.

(173) Hansen, K.; Biegler, F.; Ramakrishnan, R.; Pronobis, W.; Von Lilienfeld, O. A.; Müller,

K. R.; Tkatchenko, A. Machine Learning Predictions of Molecular Properties: Accurate Many-Body Potentials and Nonlocality in Chemical Space. *J. Phys. Chem. Lett.* **2015**, *6* (12), 2326–2331. https://doi.org/10.1021/acs.jpclett.5b00831.

(174) Rogers, D.; Hahn, M. Extended-Connectivity Fingerprints. *J. Chem. Inf. Model.* **2010**, *50*, 742–754. https://doi.org/10.1021/ci100050t.

(175) Zhang, Z.; Wang, Y.-G. Molecular Design of Dispersed Nickel Phthalocyanine@Nanocarbon Hybrid Catalyst for Active and Stable Electroreduction of CO 2. *J. Phys. Chem. C* **2021**, *125*, 13836–13849. https://doi.org/10.1021/acs.jpcc.1c02508.

(176) Weininger, D. SMILES, a Chemical Language and Information System: 1: Introduction to Methodology and Encoding Rules. *J. Chem. Inf. Comput. Sci.* **1988**, *28* (1), 31–36. https://doi.org/10.1021/CI00057A005.

(177) Schultz, J.; Milpetz, F.; Bork, P.; Ponting, C. P. SMART, a Simple Modular Architecture Research Tool: Identification of Signaling Domains. *Proc. Natl. Acad. Sci.* **1998**, *95* (11), 5857–5864. https://doi.org/10.1073/PNAS.95.11.5857.

(178) Prykhodko, O.; Johansson, S. V.; Kotsias, P. C.; Arús-Pous, J.; Bjerrum, E. J.; Engkvist, O.; Chen, H. A de Novo Molecular Generation Method Using Latent Vector Based Generative Adversarial Network. *J. Cheminform.* **2019**, *11* (1), 1–13. https://doi.org/10.1186/s13321-019-0397-9.

(179) Elton, D. C.; Boukouvalas, Z.; Fuge, M. D.; Chung, P. W. Deep Learning for Molecular Design—a Review of the State of the Art. *Mol. Syst. Des. Eng.* **2019**, *4* (4), 828–849. https://doi.org/10.1039/C9ME00039A.

(180) Krenn, M.; Häse, F.; Nigam, A.; Friederich, P.; Aspuru-Guzik, A. Self-Referencing Embedded Strings (SELFIES): A 100% Robust Molecular String Representation. *Mach. Learn. Sci. Technol.* **2019**, *1* (4), 045024. https://doi.org/10.1088/2632-2153/aba947.

(181) Montavon, G.; Rupp, M.; Gobre, V.; Vazquez-Mayagoitia, A.; Hansen, K.; Tkatchenko, A.; Müller, K. R.; Anatole Von Lilienfeld, O. Machine Learning of Molecular Electronic Properties in Chemical Compound Space. *New J. Phys.* **2013**, *15* (9), 095003. https://doi.org/10.1088/1367-2630/15/9/095003.

(182) Montavon, G.; Hansen, K.; Fazli, S.; Rupp, M.; Biegler, F.; Ziehe, A.; Tkatchenko, A.; Anatole Von Lilienfeld, O.; Müller, K.-R. *Learning Invariant Representations of Molecules for Atomization Energy Prediction*; 2012; Vol. 25. https://doi.org/10.5555/2999134.2999184.

(183) Alexopoulos, K.; Wang, Y.; Vlachos, D. G. First-Principles Kinetic and Spectroscopic Insights into Single-Atom Catalysis. **2019**. https://doi.org/10.1021/acscatal.9b00179.

(184) Bjerrum, E. J. *SMILES Enumeration as Data Augmentation for Neural Network Modeling of Molecules*.

(185) Iovanac, N. C.; Savoie, B. M.; Davidson, C. D. Improved Chemical Prediction from Scarce Data Sets via Latent Space Enrichment. *J. Phys. Chem. A* **2019**, *123*, 4295–4302. https://doi.org/10.1021/acs.jpca.9b01398.

(186) Rochelle, G.; Chen, E.; Freeman, S.; Van Wagener, D.; Xu, Q.; Voice, A. Aqueous Piperazine as the New Standard for CO2 Capture Technology. *Chem. Eng. J.* **2011**, *171* (3), 725–733. https://doi.org/10.1016/j.cej.2011.02.011.

(187) Boot-Handford, M. E.; Abanades, J. C.; Anthony, E. J.; Blunt, M. J.; Brandani, S.; Mac Dowell, N.; Fernández, J. R.; Ferrari, M. C.; Gross, R.; Hallett, J. P.; et al. Carbon Capture and Storage Update. *Energy Environ. Sci.* **2013**, *7* (1), 130–189. https://doi.org/10.1039/C3EE42350F.

(188) Rochelle, G. T. Amine Scrubbing for CO2 Capture. *Science (80-.).* **2009**, *325* (5948), 1652–1654. https://doi.org/10.1126/science.1176731.

(189) Bard, A. J.; Faulkner, L. R. *Electrochemical Methods: Fundamentals and Applications*, 2nd ed.; Wiley, 2001.